A computational model of intrathalamic signaling via open-loop thalamo-reticular-thalamic architectures

Jeffrey W. Brown[1], Aynaz Taheri[2], Robert V. Kenyon[2], Tanya Berger-Wolf[2], and Daniel A. Llano[1,3,4,5]

1. University of Illinois College of Medicine at Urbana-Champaign, Urbana, IL 61801
2. Department of Computer Science, University of Illinois at Chicago, Chicago, IL 60607
3. Beckman Institute for Advanced Science and Technology, University of Illinois at Urbana-Champaign, Urbana, IL 61801
4. Neuroscience Program, University of Illinois at Urbana-Champaign, Urbana, IL 61801
5. Department of Molecular and Integrative Physiology, University of Illinois at Urbana-Champaign, Urbana, IL 61801

Corresponding Author:
Daniel Llano, M.D., Ph.D.
2355 Beckman Institute
405 North Mathews Avenue
Urbana, IL 61801
d-llano@illinois.edu
(217) 244-0740

Abstract:

The thalamic reticular nucleus (TRN), a sheet of GABAergic neurons that partially envelops, receives excitatory input from, and projects inhibitory output to the dorsal thalamus, is known to form part of the thalamus' intrinsic connectivity. In this capacity, the TRN has been shown to play a critical role in shaping physiological phenomena such as spindle-wave and absence-seizure activity, while it is also speculated to contribute to integrative neural functions such as arousal and attention. It was long supposed that pairs of thalamic relay (TC) and TRN neurons formed "closed" disynaptic loops, in which a TC neuron was inhibited by the TRN neuron it excited. Recent experimental observations and modeling studies, however, support both the existence and potential functional significance of "open-loop" thalamo-reticulo-thalamic (TC-TRN-TC) synaptic motifs, in which neurons from the TRN are not reciprocally excited by the TC neurons they inhibit. We hypothesized that these structural modules, when connected in series, might underlie certain modes of signal propagation from one part of the thalamus to another. In the present study, we sought to evaluate the relative capacities of closed- and open-loop TC-TRN-TC synaptic configurations to support both stimulus-evoked propagation and oscillation, both of which characterize a variety thalamic and thalamocortical waveforms, while simultaneously exploring the possibility that synaptic connections exclusive to the TRN, of which both chemical or electrical varieties have been identified, might cooperatively or separately underlie these wave properties. To this end, we generated and simulated permutations of a small thalamo-reticular-cortical network, allowing select synapses to vary both by class (homogeneously) and independently (heterogeneously), and examined how synaptic variations altered the propagative and oscillatory properties of the stimulus-driven responses arising in the networks. Our analysis revealed that 1) stimulus-evoked signal propagation was best supported in networks possessing strong open-loop TC-TRN-TC connectivity; 2) oscillation arose most commonly though one of two mechanisms, one of which involved periodically occurring post-inhibitory rebound induced by the TRN in the thalamus and required strongly closed-loop TC-TRN-TC motifs and the other of which was characterized by the propagation of oscillatory activity across a network and was dependent on uniformly strong reticulothalamic synapses; 3) intrareticular synapses were neither primary substrates of propagation nor oscillation, tending to interfere with the former and either attenuating or

facilitating a weak, nondominant form of the latter; 4) neither the average propagative nor oscillatory efficiency of those network permutations best accommodating these properties significantly changed as a function of altering the duration of a fixed, external stimulus applied to them; and 5) heterogeneously synaptic networks tended to support more robust oscillation than their homogeneous counterparts, while the capacity to support propagation did not depend on the spatial uniformity synaptic weights. We relate these findings to those elucidated by related modeling studies constructed around exclusively closed-loop TC-TRN-TC connectivity and discuss the functional implications of both thalamic architectures relative to experimental data concerning normal and pathological processes in the thalamus.

Significance Statement:

Interactions between the dorsal thalamus, which functions as a relay for sensory, motor, and integrative information from subcortical brain structures to the cerebral cortex, and thalamic reticular nucleus (TRN) are known to underlie various neurophysiological waveforms and are speculated to contribute to phenomena such as arousal, attention, sleep, and epileptic processes. Despite this, the synaptic microarchitectures forming the basis for dorsal thalamus-TRN interactions are not fully understood. The computational neural model we present in this manuscript is among the first to incorporate so-called "open-loop" thalamo-reticular-thalamic (TC-TRN-TC) synaptic motifs, which have been experimentally verified in both anatomical and physiological studies. We elucidate how open-loop motifs possess the capacity to shape the propagative and oscillatory properties of signals intrinsic to the thalamus and evaluate the wave dynamics they support relative to closed-loop TC-TRN-TC pathways and intrareticular synaptic connections. Our model also generates predictions regarding how different spatial distributions of reticulothalamic and intrareticular synapses affect these signaling properties.

Introduction:

The thalamus has long been regarded as the "relay station" of the brain, through which most sensory information travels to reach dedicated areas of the cerebral cortex. While pathways between the thalamus and cortex have been extensively studied, both structurally and functionally, the nature and functional significance of intrathalamic pathways and signal propagation represent outstanding questions. Monosynaptic connections between thalamic relay (thalamocortical; TC) neurons are not believed to exist abundantly within the mature mammalian brain (Smith et al., 2006; Lee et al., 2010), and while inhibitory interneurons found in thalamic nuclei of certain mammalian species project to TC neurons (Guillery and Sherman, 2002; Sherman, 2004), there is no evidence that these interneurons participate in disynaptic pathways between TC neurons.

In fact, the major intermediary allowing for communication between thalamic relay neurons, the thalamic reticular nucleus (TRN), is extrinsic to the thalamic nuclei in which these neurons reside. The TRN is a sheet of GABAergic neurons in the ventral thalamus that partially envelops the dorsal thalamus (typically considered the "thalamus proper," in which all first- and higher-order thalamic nuclei are found; Pinault, 2004). Although the TRN was identified in the late 19th Century and has been recorded from extensively in slice preparations, a dearth of *in vivo* recordings owing to the TRN's deep position within the brain has left a lack of definitive information on the structure's integrative functional significance; the structure has, however, been speculated to participate in phenomena ranging from selective attention (Crick, 1984; Guillery et al., 1998; McAlonan et al., 2006) to sleep and arousal (Llinás and Paré, 1991; Steriade et al., 1993), and may also play a role in generating certain kinds of seizures (von Krosigk et al., 1993; Bal et al., 1995; Destexhe et al., 1996a; Huguenard, 1998; McCormick and Contreras, 2001) and neurodevelopmental disorders (Wells et al., 2016; Krol et al., 2018). The TRN projects exclusively to TC neurons of the dorsal thalamus, with the former functioning as the latter's primary source of inhibition and, consequently, as a putative filter of thalamocortical signaling (Sherman and Guillery, 2001). Reciprocal, glutamatergic thalamoreticular (TC-TRN) connections are also known to exist, with the bidirectional communication between the dorsal thalamus and TRN thought to form the minimal network

necessary for the generation and propagation of sleep spindles, a waveform endemic to stage 2 NREM sleep (Steriade and Deschênes, 1984; Steriade et al., 1987; von Krosigk et al., 1993; Bal et al., 1995; Kim et al., 1995; Ulrich and Huguenard, 1997).

The structural constitution of bidirectional pathways connecting the dorsal thalamus and TRN has been the subject of ongoing debate. It was originally assumed that thalamo-reticulo-thalamic (TC-TRN-TC) pathways were reciprocal in nature, forming "closed loops" of recurrent inhibition delivered to TC neurons (Fig. 1A, left; Hale et al., 1982; Steriade et al., 1993; Warren et al., 1994; Sherman and Guillery, 1996; Pinault, 2004). While closed disynaptic loops have indeed been confirmed with *in vivo* and *in vitro* electrophysiological studies in both the rat and cat thalamus, they were only identified in a minority of examined TC-TRN pairs (Shosaku, 1986; Lo and Sherman, 1994; Gentet and Ulrich, 2003; Pinault, 2004); these observations were consistent with anatomical tracing studies in both species (Pinault and Deschênes, 1998; FitzGibbon et al., 2000). Another connectional scheme between the dorsal thalamus and TRN is the so-called "open-loop" TC-TRN-TC pathway, wherein a TC neuron is not reciprocally inhibited by the TRN neuron it excites (Fig. 1A, right); within the thalamus, this disynaptic motif functions as a substrate for lateral inhibition. Open-loop configurations have been inferred from recordings in rodent thalamic slice preparations (Crabtree et al., 1998; Crabtree and Isaac, 2002; Lam and Sherman, 2005; Lee et al., 2010; Lam and Sherman, 2015) and identified in anatomical labeling studies (Pinault and Deschênes, 1998; Kimura et al., 2007; Kimura, 2014). Furthermore, open-loop pathway variants in the form of X-TRN-TC are also known to exist, with X representing potentially indirect sources of modulation to the sensory thalamus via the TRN, such as monoaminergic and cholinergic brainstem nuclei, nuclei of the basal forebrain, amygdala, and multimodal association cortex (Asanuma and Porter, 1990; Bickford et al., 1994; Zikopoulos and Barbas, 2006; Sun et al., 2013; Pita-Almenar et al., 2014).

Several computational models simulating either thalamic (Destexhe et al., 1993; Destexhe et al., 1994; Golomb et al., 1996; Destexhe et al., 1996a; Sohal and Huguenard, 1998; Bazhenov et al., 1998;

Wasylenko et al., 2010; Pham and Haas, 2018) or thalamocortical networks (Destexhe et al., 1998; Bazhenov et al., 2002; Traub et al., 2005; Izhikevich and Edelman, 2008; Rogala et al., 2013) and incorporating closed-loop TC-TRN-TC pathways have reproduced propagative and/or oscillatory waveforms intrinsic to the thalamus with high fidelity, including sleep spindles, epileptiform activity, and gamma oscillations, and have engendered important dynamical clarifications or experimentally verifiable predictions in relation to these phenomena. In a departure from these computational studies and in an effort to explore the effects of thalamocortical transmission within an open-loop thalamoreticular system, our research group previously simulated a one-dimensional, three-neuron thalamo-reticulo-cortical computational network, in which a TRN neuron projected to a TC neuron non-reciprocally (i.e., in an open-loop manner), with both the TC and TRN neurons receiving stochastic external input (Willis et al., 2015). We reported that the open-loop TC-TRN-TC pathway, rather than uniformly depressing thalamic (and consequently cortical) activity, paradoxically enhanced thalamocortical output over a domain of TC and TRN input frequencies. This demonstrated the capacity of an open-loop system to function as a tunable filter of thalamocortical transmission, subject to the temporal dynamics of input to the TRN, whether from other, non-reciprocally connected TC neurons or extrinsic sources. In both our previous model and earlier models built on closed-loop TC-TRN-TC synaptic motifs, the post-inhibitory rebound (PIR) exhibited by TC neurons, as mediated by T-type Ca^{2+} channels and driven by inhibition from the TRN, served as a catalyst of signal propagation within the networks: in the case of the open-loop network, PIR could enhance vertical (thalamocortical) transmission, while in closed-loop networks, it could drive both horizontal (intrathalamic) and vertical signal propagation (Destexhe et al., 1993; Golomb et al., 1996; Destexhe et al., 1996a; Destexhe et al., 1998; Sohal and Huguenard, 1998; Bazhenov et al., 1998; Bazhenov et al., 2002; Traub et al., 2005; Rogala et al., 2013; Willis et al., 2015; Pham and Haas, 2018). In physiological studies, TRN-driven PIR has been observed to promote thalamic bursting behavior (von Krosigk et al., 1993; Sherman, 2001; Halassa et al., 2011).

Based on previous physiological characterizations and computational modeling of open-loop TC-TRN-TC synaptic organization, we hypothesized that these synaptic modules might underlie intrathalamic

signal propagation. Accordingly, we sought in the present study to test this hypothesis, specifically evaluating the efficacy of open-loop pathways relative to other potential synaptic configurations in mediating signal transmission across the thalamus. To this end, we constructed a baseline model network based on that of Willis et al. (2015) by connecting in series three thalamo-reticulo-cortical (layer 4) pathways, or TC-TRN-L4 "columns," potentially featuring either or both closed- and open-loop TC-TRN-TC motifs, with the latter constituting one mode of connectivity between parallel TC-TRN-L4 columns. Intrareticular synapses represented the other structural connections between columns, based on the identification of both GABAergic (Ahlsén and Lindström, 1982; Steriade et al., 1990; Cox et al., 1996; Sanchez-Vives et al., 1997; Shu and McCormick, 2002; Deleuze and Huguenard, 2006; Lam et al., 2006) and electrical synapses (Landisman et al., 2002; Long et al., 2004; Fuentealba et al., 2004; Deleuze and Huguenard, 2006; Lam et al., 2006) between TRN neurons. Thus, we included three different polysynaptic, intercolumnar pathway configurations in our network (Fig. 1B, from left to right): 1) those with a central chemical intrareticular synapse; 2) those with a central electrical intrareticular synapse; and 3) open-loop TC-TRN-TC pathways.

To analyze how each variety of intercolumnar pathway contributed to network dynamics, permutations of the baseline network were generated by varying three properties associated with each of the intercolumnar synaptic motifs: 1) the conductance of GABAergic TRN-TRN synapses; 2) the electrical coupling coefficient between TRN neurons; and 3) a TC-TRN-TC "openness" coefficient that corresponded to the ratio of lateral to recurrent reticulothalamic connections within the network. In an effort to account for the varying degrees of spatial uniformity with which intrareticular and TC-TRN-TC synaptic architectures might be distributed within the thalamus, the synaptic parameters were varied in one of two manners: 1) homogeneously, whereby parameters were varied systematically within each variable synaptic class and across a range of discrete physiological values, or 2) heterogeneously, where parameters varied discretely for every individual intracolumnar synapse and in which the TC-TRN-TC openness coefficient was replaced by the conductances of individual reticulothalamic (TRN-TC) synapses. We quantified network dynamics as a function of variable TC-TRN-TC and intrareticular synaptic architectures by defining and

190 measuring two properties inherent to stimulus-evoked responses in each network variant: propagation and
191 oscillation, with the latter included in light of the fact that many characterized thalamic waveforms both
192 oscillate and propagate through the thalamus (Sherman and Guillery, 2001). We furthermore compared
193 the relative capacities of homogeneous and heterogeneous network permutations to support these
194 properties.
195
196 **Computational Model and Methods:**
197 *Intrinsic neuronal models*
198 Our network model was directly based on an earlier incarnation published by our research group (Willis
199 et al., 2015). Single-compartment TC, TRN, and cortical (L4) model neurons obeyed Hodgkin-Huxley
200 kinetics, with membrane potentials V varying according to the first-order differential equation
201 $$C\frac{dV}{dt} = -g_L(V - E_L) - \sum_i g_i(V)(V - E_i) \quad (1)$$

202 where C is the membrane capacitance, g_L and E_L are the leakage conductance and reversal potential,
203 respectively, and $g_i(V)$ and E_i are the dynamic conductance and reversal potential, respectively, of the ith
204 voltage-gated, ligand-gated (chemical synaptic), or electrical synaptic conductance (for electrical synaptic
205 conductances, the effective reversal potential is equal to the presynaptic membrane potential; see
206 Equation 2a). All three varieties of model neurons expressed both the standard transient sodium (I_{Na}) and
207 delayed-rectifier potassium (I_K) currents, as reported by Willis et al. (2015). TC and TRN neurons
208 additionally included a T-type calcium conductance (t-current; I_T) and hyperpolarization-activated cation
209 current (h-current; I_H), following the TC model of Deleuze et al. (2012). Both TRN and L4 cells
210 expressed a slow, non-inactivating potassium conductance (I_M), following the modeling of Pospichil et al.
211 (2008), which accounts for the spike-frequency adaptation previously reported in physiological recordings
212 from these neurons (Yamada et al., 1989; Willis et al., 2015). A list of intrinsic model cell parameters,
213 including current conductances, reversal potentials, selected gating kinetics, and membrane capacitance,
214 can be found in Table 1.
215

Synaptic models

The kinetics of chemical synapses in our model network conformed to the synaptic depression model of Tsodyks and Markram (1997; Tsodyks et al., 1998), following our previous computational network model (Willis et al., 2015). The Tsodyks and Markram model presupposes a finite quantity of "resources," akin to synaptic vesicles, capable of being released by the presynaptic neuron; these resources can exist in an active, inactive, or recovered state. A parameter U_{SE} characterizes the fraction of recovered resources that can be converted to an active state (i.e., for release by the presynaptic neuron) following action potential induction in the presynaptic axon terminal(s). Following resource activation, synapses inactivate according to the time constant τ_{inact}; resources become available again for activation after a recovery period described by the time constant τ_{recov}. These parameters, along with the neurotransmitters, postsynaptic conductances, and reversal potentials characterizing all of the chemical synapses in our model, are given in Table 2.

Glutamatergic thalamoreticular and thalamocortical (TC-L4) and baseline GABAergic reticulothalamic synaptic parameters matched those of our earlier model (Willis et al., 2015), with the latter synapses allowed to vary in conductance (see the *Network architecture and permutations* subsection for additional details). TRN-TC signaling was mediated exclusively through $GABA_A$ receptors, mirroring other thalamic and thalamocortical models in which the slower TRN-TC $GABA_B$ conductance was omitted (Traub et al., 2005; Rogala et al., 2013; Willis et al., 2015; Pham and Haas, 2018). Both GABAergic ($TRN\text{-}TRN_{GABA}$) and electrical synapses ($TRN\text{-}TRN_{Elec}$) were included between TRN neurons; as with TRN-TC synapses, both varieties of TRN-TRN synapses were allowed to vary in strength. Although evidence has been presented challenging the existence of GABAergic intrareticular synapses in certain mammalian species and age groups (Pinault et al., 1997; Landisman et al., 2002; Pinault, 2004; Cruikshank et al., 2010; Hou et al., 2016), our model avoided making assumptions regarding their presence, strength, or spatial distribution by allowing the associated synaptic conductances to vary over a range of physiological values, including zero, and in distribution.

Electrical synapses between TRN neurons were based on the Cx36-dependent intrareticular gap junctions first identified by Landisman et al. (2002). For TRN neurons, the sum of electrical synaptic currents (I_{Elec}) entering any postsynaptic neuron *j* from presynaptic neurons *i* was included in the rightmost term from Equation 1 and calculated as

$$I_{Elec(j)} = \sum_i g_{ij} \left(V_j - V_i\right) \quad (2a)$$

where g_{ij} was itself calculated as

$$g_{ij} = D(x) \frac{g_{gap}}{1/_{CC} - 1} \quad (2b)$$

where *CC* was the electrical coupling coefficient between TRN neurons *i* and *j*, g_{gap} is the gap junction conductance (set at 5 nS), and *D(x)* was a scaling factor that depended on the physical distance between the coupled TRN neurons (see the *Network architecture and permutations* subsection for additional details; Dayan and Abbott, 2005; Traub et al., 2005; Shimizu and Stopfer, 2013). TRN-TRN_{Elec} were symmetrical (non-rectifying), such that G_{ij}=G_{ji}.

A generalized afferent synaptic input was delivered to every TC neuron in the model. Given that the temporal profiles of both spontaneous and stimulus-evoked inputs impinging on the dorsal thalamus can vary drastically from moment to moment, these external inputs were delivered as Poisson-modulated spike trains centered at 40 Hz; the central frequency was chosen to maximize thalamocortical output relative to the saturation of the external synapse and concurrent inhibitory input being received from the TRN (Willis et al., 2015). Individual pulses lasted 0.1 ms. An additional high-frequency pulse train was inserted into neuron TC_A over a fixed time interval during every network simulation run (see the *Computational methods and calculation of network dynamics* subsection for additional details). The reversal potential, conductance, and kinetics of these synapses were directly based on retinogeniculate synapses (Chen and Regehr, 2003), although the generic nature of the external inputs in our model allows them to represent not only immediately upstream sensory input but also brainstem modulation (e.g., serotonergic, adrenergic) known to act on thalamic nuclei (Siegel and Sapru, 2015).

Given the small spatial scale of our model (see the *Network architecture and permutations* subsection for additional details), synaptic delays associated with finite axonal conductance times within the TRN and between the TRN and dorsal thalamus were disregarded, mirroring the simplification incorporated into previous thalamic and thalamocortical models simulating synaptic interactions on the order of 100 microns (Golomb et al. 1996; Traub et al., 2005). Although small (~1 ms) thalamocortical delays were inserted into the network model of Traub et al. (2005), these were likewise omitted on the basis of the cortex functioning solely as an output layer in our model. A table containing the conductances, reversal potentials, and gating kinetics for synaptic currents and further details thereof may be found in SI: Materials and Methods.

Network architecture and permutations

We constructed a 3 x 3-neuronal network comprising three interconnected thalamo-reticulo-cortical columns for use in this study (Fig. 2A). Thalamic, reticular, and cortical cell layers were aligned with one another topographically, such that TC_A projected to both TRN_A and $L4_A$ (Jones, 1975; Destexhe et al., 1998; Sohal et al., 2000; Sherman and Guillery, 2001; Pinault, 2004). The TC-TRN and TRN-TC synapses in our model were strictly local and minimally divergent (or non-divergent, in the case of TC-TRN synapses) in order to preserve disynaptic TC-TRN-TC open-loop motifs and analyze the signal propagation they may support; see the Discussion section for an elaboration of this point. Both varieties of intrareticular synapse, by contrast, were allowed to diverge, targeting both adjacent and non-adjacent TRN neurons. We extrapolated the attenuation of intrareticular synaptic strength as a function of intracellular distance based on mappings of intrinsic connections within the TRN along a horizontal (anteroposterior) plane assembled by Deleuze and Huguenard (2006). Assuming 1) an intracellular distance of 50 μm between adjacent TRN neurons, 2) a distance x (in multiples of 50 μm) between non-adjacent neurons, and 3) a Gaussian falloff in synaptic strength (Sohal and Hueguenard, 2000), the baseline (adjacent-neuron) conductances of $TRN\text{-}TRN_{GABA}$ and $TRN\text{-}TRN_{Elec}$ synapses were scaled for non-adjacent synapses using the function

$$D(x) = e^{-\frac{x^2}{2\lambda^2}} \quad (3)$$

where λ_{GABA}=531 μm and λ_{Elec}=130 μm.

In the case of so-called homogeneously synaptic network permutations, the conductances or coupling coefficients associated with three classes of synapses were allowed to vary discretely and uniformly within their class, with all external, TC-TRN, and TC-L4 synaptic conductances held constant: 1) TRN-TRN_{GABA} synapses ranged in conductance between 0 and 450 nS in steps of 50 nS; 2) TRN-TRN_{Elec} synapses ranged in coupling coefficient between 0 and 0.36 in steps of 0.06; and 3) a TC-TRN-TC "openness" coefficient, defined as the weight distribution of lateral (open-loop, comprising 2 synapses of the form $TRN_i \rightarrow TC_{i+1}$) vs. recurrent (closed-loop, comprising 3 synapses of the form $TRN_i \rightarrow TC_i$) reticulothalamic connectivity, varied between 0 (completely closed-loop) and 1.0 (completely open-loop) in steps of 0.1 (e.g, with a baseline TRN-TC conductance of 80 nS, a network with a TC-TRN-TC openness coefficient of 0.7 would set the conductance of all laterally inhibitory TRN-TC synapses at 56 nS and all recurrently inhibitory TRN-TC synapses at 24 nS). Accordingly, 10 (TRN-TRN_{GABA}) x 7 (TRN-TRN_{Elec}) x 11 (TC-TRN-TC) or 770 homogeneous network variants were generated.

For the heterogeneously synaptic network variants, all TRN-TRN and TRN-TC synapses (6 TRN-TRN_{GABA} + 3 TRN-TRN_{Elec} + 5 TRN-TC) were allowed to vary discretely and independently of one another, with all other synaptic weights held constant. Here, TRN-TRN_{GABA} synapses ranged in conductance between 0 and 400 nS in steps of 100 nS, TRN-TRN_{Elec} synapses ranged in coupling coefficient between 0 and 0.36 in steps of 0.12, and TRN-TC synapses (both laterally and recurrently inhibitory) ranged in conductance between 0 and 80 nS in steps of 16 nS. Due to both computational and time constraints, approximately 12,600 heterogeneous network permutations out of a theoretical >7 billion were generated at random. For both homogeneous and heterogeneous network variants, domains for each of the three synaptic variables were selected to include the range of conductance or coupling strengths reported in physiological measurements and/or used in similar neural models (Destexhe et al.,

1996a; Destexhe et al., 1998; Sohal and Hueguenard, 1998; Sohal et al., 2000; Landisman et al., 2002; Long et al., 2004; Traub et al., 2005). For both varieties of TRN-TRN synapse, we modestly extended the upper bounds of the synaptic parameter domains to capture a broader range of dynamics potentially generated by intrareticular synapses in the thalamoreticular system.

Computational methods and calculation of network dynamics

Our model was coded, simulated, and analyzed in MATLAB R2018b (MathWorks), utilizing both a Dell Inspiron 3847 and Hewlett-Packard Z840 running Windows 10 and nodes on the Illinois Campus Cluster (National Center for Supercomputing Applications, University of Illinois at Urbana-Champaign). Simulations employed 0.1-ms time steps, with temporal integration based on the hybrid analytic-numeral integration method of Moore and Ramon (1974), which optimizes between accurate solutions to Hodgkin-Huxley and synaptic models and computational efficiency. Statistical analysis was performed in both MATLAB and R (R Core Team, 2013), with the *glmnet* package (Friedman et al., 2010) utilized within the latter platform to perform regression analyses. Multiple linear regression was employed to establish rudimentary relationships between synaptic classes (homogeneously synaptic networks) or individual synapses (heterogeneously synaptic networks) and each of the two studied network properties, even in instances where these relationships deviated from linearity. Second-order regression models with interaction terms elucidated how synaptic interactions and nonlinearities affected these network properties. Regressions were optimized using elastic net regularization, with the specific regularization hyperparameter α selected to minimize each regression model's root-mean-square error (RMSE). To convey the relative influence of different synaptic classes or individual synapses on dynamic network properties, all regression coefficients are reported here as normalized to the coefficient with the largest absolute value; the effects corresponding to normalized regression coefficients (NRCs) with absolute values of less than 0.05 were disregarded as negligibly influential on network dynamics. Both paired Student *t*-tests and one-way analysis of variance (ANOVA) models were used to compare the mean property scores between different sets of networks, with Tukey's honestly significant difference tests used

to ascertain pairwise difference between groups in the latter. Kolmogorov-Smirnov and Levene's tests were employed to confirm normality and homogeneity of variance, respectively, when utilizing parametric mean-comparison tests; data were log-transformed as needed to conform to these prerequisites.

Individual simulations of network activity lasted either 1.000 or 1.500 s. During every run of the 1.000-s simulations, a 200-Hz spike train lasting 50 ms and beginning at the 400-ms time index was inserted at the external synapse to TC_A (fixed, "punctate" stimulation; Fig. 2B). During 1.500-s simulation runs, an extended version of the same spike train lasting 1.100 s was delivered externally to TC_A (fixed, "sustained" stimulation; Fig. 2C). These high-frequency, time-locked stimuli were modeled on those used to elicit spindle-like waves in a ferret thalamoreticular slice preparation (Kim et al., 1995; Bal et al., 1995) and designed to allow for the averaging of responses within a given network permutation across simulation runs, with variations in neuronal responses from one run to the next arising due to the stochastic (Poisson-modulated) input delivered to every TC neuron. Homogeneously synaptic networks were simulated for both 1.000 s and 1.500 s, while heterogeneously synaptic networks were simulated for 1.500 s. All simulations commenced with a 200-ms equilibration period, during which no external stimulation was delivered to TC neurons; this allowed all network elements to attain steady-state conditions.

To analyze the properties of propagation and oscillation inherent to a network's stimulus-driven response, every network permutation was simulated 1,000 times. A given network's output across these simulations, as represented by action potentials in the L4 layer of the model, was compiled by assembling spike histograms consisting of 10-ms bins for every L4 neuron (Fig. 3). Both dynamic network properties were defined relative to the most downstream element of the cortical output layer, $L4_C$. Propagation across a network was quantified as the amplitude of the initial stimulus-evoked response in the detrended $L4_C$ histogram. Because response propagation across the L4 subnetwork was consistently linear, the initial response in $L4_C$ could be predictably observed within a small, fixed interval relative to the onset of

stimulation (see the Results section for additional information on signal propagation velocities). The degree of oscillation supported by each network permutation was defined as the amplitude of the first off-center peak in the normalized autocorrelogram of post-stimulation activity (i.e., activity measured between 400 ms and 1500 ms) in the detrended $L4_C$ histogram; this corresponded to the degree to which activity in $L4_C$ was able to periodically recur. (Note that although other simulated neurons exhibited oscillatory activity as well, the term "oscillation" henceforth refers explicitly to oscillation in $L4_C$ as defined above, unless otherwise stated.) Both propagation and oscillation scores are reported as normalized to the maximum scores tabulated for each property across all the homogeneously and heterogeneously synaptic networks simulated in the study.

Results:

Response of homogeneously synaptic models to a fixed, punctate stimulus

Delivering a fixed, punctate external stimulus to TC_A was adequate to elicit strong propagative responses within a subset of homogeneously synaptic network permutations. Signals propagated linearly across the length of networks, with stimulus-evoked responses occurring at average fixed intervals of 102.29 ± 0.51 ms (mean ± standard error of the mean) between adjacent TC-TRN-L4 columns and with a mean velocity of 0.49 mm/s, assuming a 50 μm separation between adjacent neurons in each network layer.

All 770 homogeneous network variants were ranked according to their propagation scores (Fig. 4A, top). Linear regression analysis (R^2=0.829, RMSE=0.042, p<0.0001) demonstrated a strong positive correlation between the TC-TRN-TC openness coefficient and propagation scores (normalized regression coefficient or NRC=1.000), with propagation better supported in networks with stronger open-loop TC-TRN-TC pathways. By contrast, propagation tended to be modestly diminished as a function of increasing both chemical and electrical TRN-TRN synaptic connectivity (NRC=-0.135 and NRC=-0.193, respectively). Mechanistically, we interpreted this result to indicate that intrareticular synapses tended to interfere with the spike timing necessary for linear signal propagation via the open-loop TC-TRN lattice through which

they primarily traveled. Thus, the homogeneously synaptic network permutations that best accommodated signal propagation were generally ones with weak or absent synapses between TRN neurons and strong open-loop TC-TRN-TC connections. A second-order multiple regression model of propagation as a function of all three synaptic class variables (R^2=0.863, RMSE=0.039, p<0.0001) revealed a significant but small negative interaction term between TRN-TRN_{Elec} synapses and TC-TRN-TC openness (NRC=-0.239), indicating that in networks where both electrical synapses were strong and TC-TRN-TC openness high, the extent of supported propagation diminished nonlinearly. A positive interaction of comparable magnitude between chemical and electrical intrareticular synapses (NRC=0.226) tempered the negative linear effects that these two synaptic classes exerted on propagation in networks where TRN-TRN interaction was strong. No other non-negligible interaction terms with NRCs were revealed by the second-order regression model, and all the terms therein were qualitatively consistent with those in the linear regression model (Table 3). Moreover, the relative magnitude of the coefficients in the second-order regression model indicated that linear synaptic effects tended to dominate over nonlinear effects across the domains of studied synaptic weights. The mean propagation score for all networks was 0.648 ± 0.006, with scores ranging from 0.435 to 0.923.

Two network permutations exhibiting fully open-loop TC-TRN-TC connectivity (openness coefficient or OC=1.0), in which propagation was generally robust, were selected for further analysis (these networks are labeled in Figs. 4A, top, and 4B, left). Each network was indexed by its synaptic variables ([TRN-TRN_{GABA} conductance (in nS), TRN-TRN_{Elec} coupling coefficient, TC-TRN openness coefficient]): Network a ([0,0,1.0]) and Network b ([450,0.36,1.0]). The propagation score of Network a, 0.913, was the 2nd highest of the 770 ranked networks, with Network b scoring 0.757 (89th). Consistent with regression analysis, the extent of response propagation in fully open-loop networks (i.e., OC=1.0) was maximal when TRN-TRN synapses, both chemical and electrical, were absent, with increasing electrical coupling between TRN neurons attenuating propagation more rapidly than increasing GABAergic projection strength (Fig. 4B, left). Voltage traces of all network neurons depict activity, both preceding and

following fixed, punctate external stimulation of TC_A (yellow arrows), during representative 1.0-s simulations of Networks a and b (Fig. 4C, left and center). Both isolated spikes and bursts, defined as at least three spikes occurring in rapid succession, were observed intermittently in neurons found in all three network layers. In Network a, stimulus-evoked activity tended to propagate smoothly from TC_A to TC_C; near-synchronous propagation cascades were elicited in both the TRN and L4 layers of the model, having been stimulated by propagating activity in upstream TC neurons. Smooth, linear propagation of action potentials across the network depended on the synchronous induction of inhibitory postsynaptic potentials (IPSPs) and the ensuing post-inhibitory rebound spikes in TC neurons, which occurred reliably and at fixed intervals in Network a due to both its fully open-loop TC-TRN-TC connectivity and the absence of any synapses within the network's TRN layer. Relative to Network a, Network b was not capable of supporting activity propagation with the same fidelity, as predicted by the regression analyses. Mechanistically, this was attributable to both the presence of strong TRN-TRN_{GABA} synaptic connections, which reduced the incidence of IPSPs in TC neurons required for signal propagation across the network, and Network b's strong electrical coupling between TRN neurons, which destructively shunted a propagating signal away from the thalamoreticular lattice through which it predominantly traversed the network.

Propagation and oscillation scores across all 770 homogeneous networks, as driven by a fixed, punctate stimulus, were strongly anticorrelated (Pearson's r=-0.739, p<0.0001). Accordingly, oscillation was best accommodated in network permutations exhibiting strongly closed-loop connectivity (Fig. 4A, bottom), as confirmed quantitatively through a linear regression model in which TC-TRN-TC openness was associated with an NRC of -1.000 (R^2=0.661, RMSE=0.137, p<0.0001). This analysis furthermore demonstrated that both varieties of TRN-TRN synapse played nearly negligible roles in mediating or otherwise modulating oscillation, yielding NRCs of 0.058 and 0.064 for TRN-TRN_{GABA} and TRN-TRN_{Elec} synapses, respectively. The insignificant relationship between oscillation and the weights of intrareticular synapses was further reflected by the largely unpatterned distribution of oscillation scores in TRN-TRN_{GABA} x TRN-TRN_{Elec} phase space for the 70 fully closed-loop network variants (Fig. 4B, right).

No significant interactions or nonlinearities were disclosed through a second-order regression model relating oscillation to the three variable synaptic classes; indeed, this model was fully consistent with and only marginally more explanatory than its linear counterpart (R^2=0.687, RMSE=0.137, p<0.0001; Table 3). The mean oscillation score across network variants in this set of simulations was 0.300 ± 0.006, with scores ranging from 0.012 to 0.758.

Although oscillation was observed in homogeneously synaptic networks driven by a fixed, punctate stimulus to TC_A, any oscillation in $L4_C$ was judged to be generally unrelated to the fixed stimulus; equivalently stated, stimulus-induced oscillatory activity induced in $L4_A$ did not propagate well through the network to $L4_C$. This deduction followed from the facts that 1) networks that supported robust oscillation (strongly closed-loop networks) did not facilitate strong signal propagation, and in particular, the propagation of oscillatory activity from one end of the network to the other and 2) the remaining synaptic motifs connecting adjacent columns in the network and potentially serving as substrates for signal propagation, namely those featuring a central intrareticular synapse, were demonstrated to exert generally negligible or weakly attenuating effects on network propagation and oscillation. In absence of stimulus-driven oscillatory activity propagating through the network, the default and indeed predominant mechanism by which oscillation arose in $L4_C$ was through post-inhibitory rebound in TC_C, as engendered by the strong recurrent inhibition found in network permutations exhibiting primarily closed-loop TC-TRN-TC connectivity. This mechanism of oscillation was exemplified by Network c ([50, 0.18, 0]), which received an oscillation score of 0.690 (7^{th} highest of 770 network permutations): as illustrated in a representative simulation of this network (Fig. 4C, right), an initial action potential in TC_C, elicited through a stochastic external input and notably in the absence of upstream oscillatory activity propagating through the network, drove recurrent inhibition in this neuron via TRN_C, causing oscillation in TC_C over several cycles and consequently driving concurrent oscillation in $L4_C$.

Based on the nature of oscillation in homogeneously synaptic network variants responding to a fixed, punctate stimulus, we speculate that the rate of network oscillation corresponded to the kinetics of the t-current, which underlies PIR. Across these simulations, oscillatory responses recurred linearly at mean intervals of 109.27 ± 0.31 ms, or equivalently, at a mean frequency of 9.15 ± 0.02 Hz.

Response of homogeneously synaptic models to a fixed, sustained stimulus

As was the case when homogenously synaptic networks responded to a punctate external stimulus, homogeneous network responses to a fixed, sustained stimulus propagated in a linear manner, recurring in adjacent TC/L4 neurons at averaged fixed intervals of 99.96 ± 0.69 ms and propagating at a velocity of 0.50 mm/s. All networks variants driven by a fixed, sustained external stimulus to TC_A were ranked separately according to their scores for each network property (Fig. 5A, top). Network permutations that allowed for robust propagative responses when TC_A was stimulated in a punctate manner similarly supported such responses when external stimulation to TC_A was sustained (linear regression, R^2=0.793, RMSE=0.047, p<0.0001). Propagation scores rose with increasing TC-TRN-TC openness (NRC=1.000), while GABAergic and electrical TRN-TRN synapses both tended to exert moderate attenuating effects on network propagation (NRC=-0.173 and NRC=-0.136, respectively). A second-order regression model (R^2=0.842, RMSE=0.041, p<0.0001) disclosed qualitatively similar synaptic interactions when homogeneous networks were stimulated in a sustained manner as when they were driven by a punctate stimulus (Table 4). The one exception to this was an additional though small negative interaction between TRN-TRN_{GABA} synapses and TC-TRN-TC openness (NRC=-0.152). Both this negative interaction and the one between TRN-TRN_{Elec} and TC-TRN-TC openness indicated that propagation was more significantly affected by connections in the TRN layer as a function of increasing open-loop TC-TRN-TC architecture; this is evident in Fig. 5B (left), as propagation scores conspicuously decrease in network variants with an OC of 1.0 as either chemical or electrical synapses increase in weight. The mean propagation score arising from sustained stimulation to TC_A was 0.633 ± 0.006, with scores ranging from

0.414 to 0.961; these scores were not significantly different than those associated with fixed, punctate stimulation of the same network permutations [paired *t*-test, $t(769)=1.067$, $p=0.287$].

A simulation of Network d ([0,0.06,1]) illustrates typical signal propagation in a network permutation exhibiting high open-loop TC-TRN-TC connectivity and weak intrareticular synapses responding to a fixed, sustained stimulus delivered to TC_A (Fig. 5C, left); its position as a function of propagation score is indicated in Figs. 5A (top) and 5B (left). The capacity of Network d to accommodate response propagation throughout the length of the network in response to sustained stimulation was mechanistically comparable to the similarly constituted Network a in the presence of punctate stimulation (see Fig. 4C), with the former earning a propagation score of 0.961, the highest score among all homogeneous network permutations exhibiting propagation as a function of fixed, sustained external stimulation.

Oscillatory responses in networks when subjected to fixed, sustained stimulation recurred linearly in $L4_C$ at mean intervals of 110.26 ± 0.25 ms (9.07 ± 0.02 Hz). Propagation and oscillation scores across networks were similarly anticorrelated ($r=-0.671$, $p<0.0001$), though not as strongly as when TC_A was stimulated in a fixed, punctate manner. While network permutations with stronger closed-loop TC-TRN-TC architectures were most permissive of cortical oscillation, this relationship was neither markedly linear nor monotonically decreasing as a function of increasing openness coefficient (linear regression, $R^2=0.526$, RMSE=0.145, $p<0.0001$; Table 4). Rather, a one-way ANOVA with Tukey's tests revealed that, on average, oscillation scores peaked and remained statistically indistinguishable from one another across the subset of network permutations with OCs between 0 and 0.4, with scores then decreasing in a roughly linear fashion with increasing TC-TRN-TC openness (Fig. 5D; $F(10,759)=137.8$, $p<0.0001$). This trend was partially accounted for in a second-order regression model ($R^2=0.630$, RMSE=0.129, $p<0.0001$), in which the quadratic term in TC-TRN-TC openness had an NRC of -1.000 and was thus the major determinant of network oscillation (all other synaptic variables in this model possessed NRCs with

absolute values less than 0.06). As with oscillation under the previous fixed stimulation condition, the inconsequential roles played collectively by TRN-TRN synapses in oscillation here were reflected by the haphazard distribution of scores in intrareticular synaptic parameter space (Fig. 5B, middle and right). The mean oscillation score of homogeneously synaptic networks subjected to fixed, sustained stimulation was 0.369 ± 0.006 (scores ranged from 0.006 to 0.827), with networks exhibiting a greater oscillation score under this fixed stimulation condition than when stimulated in fixed, punctate manner [paired *t*-test, $t(769)=-13.345$, $p<0.0001$].

We surmise that the discrepancy in network oscillation scores between homogeneous network variants excited in punctate and sustained manners owes to a mode of oscillation that, though still infrequently observed, became more prevalent in the latter set of simulations. Network permutations with somewhat stronger closed- than open-loop TC-TRN-TC connectivity (OCs=0.3 and 0.4), such as Network e ([100,0.12,0.4]; oscillation score, 0.662; rank, 21st of 770), were intermittently able to support the propagation of oscillatory activity from TC_A to TC_C, and thus between their downstream cortical counterparts, by virtue of 1) receiving sustained external input through TC_A in a manner sufficient to elicit linearly recurring action potentials and 2) possessing sufficiently strong laterally inhibitory TRN-TC synapses to support propagation (Fig. 5C, middle). As previously mentioned, this mechanism for generating oscillation in $L4_C$ was comparatively rarer when the same subset of networks was stimulated in a fixed, punctate manner, as oscillation in TC_A could not often be sustained without concurrent, high-frequency external stimulation. Network f ([450,0.36,0.2)] typified the still-dominant mode of oscillation exhibited in homogeneous networks stimulated in a punctate manner, namely that oscillation observed in strongly closed-loop networks deriving from PIR in TC_C (Fig. 5C, right). In the selected simulation of this network, oscillatory activity was enabled by a single epoch of signal propagation, although Poisson-mediated external input to TC_C remained the more common catalyst for this mode of oscillation. Notably, neither the presence of strong GABAergic nor electrical intrareticular synapses in Network f exerted

much effect on its ability to support oscillation (score, 0.726, 4th of 770), as predicted by the regression models.

Response of heterogeneously synaptic models to a fixed, sustained stimulus

Given both the number of individually varying synaptic parameters within heterogeneously synaptic networks (14, vs. 3 in the homogeneous networks) and the large number of heterogeneously synaptic network permutations simulated in this study (~12,600), we relied solely on regression analysis to ascertain the ultimate relationship between individual synaptic variables and network properties of interest; neither ranking network variants in order of performance nor examining specific parameter subspaces, as was done in the case of homogeneous networks, was practical. Accordingly, we constructed circuit-level schematics of linear regression models for propagation (Fig. 6A) and oscillation (Fig. 6B) as functions of the 14 synaptic variables in heterogeneous networks. While second-order regression models for both performance metrics were also generated, these models revealed only a small number of significant quadratic or interaction terms that could not more parsimoniously be accounted for by single synaptic variables in the corresponding linear regressions. We note any nonlinearities of interest here and report all regression results in Table 5.

The extent of stimulus-evoked response propagation in those heterogeneously synaptic networks generated increased chiefly as a function of increasing the strength of the more downstream of the two laterally inhibitory TRN-TC synapses, $TRN_B \rightarrow TC_C$: the corresponding term in a linear regression model of propagation (R^2=0.742, RMSE=0.069, p<0.0001) possessed an NRC of 1.000 (Fig. 6A). Propagation scores, which averaged at 0.601 ± 0.001 and ranged from 0.299 to 1.000, also scaled to a lesser extent with the more upstream laterally inhibitory reticulothalamic synapse, $TRN_A \rightarrow TC_B$ (NRC=0.608). The two inhibitory intrareticular synapses originating at the rightmost end of the model network, $TRN_C \rightarrow TRN_A$ and $TRN_C \rightarrow TRN_B$, both exerted a small negative effect on propagation (NRC=-0.087 and NRC=-0.084, respectively). Additionally, two TRN-TRN_{Elec} synapses, TRN_A=TRN_B and TRN_A=TRN_C

(where the "=" denotes an electrical synapses), marginally decremented propagation in heterogeneous networks, with NRCs of -0.051 and -0.072, respectively. These findings clarified at an individual synaptic level the observation that strong TRN-TRN interactions, whether chemical or electrical, tended to impede signal propagation in homogeneous network variants. The three recurrently inhibitory synapses also decremented propagation efficiency to minor degrees, with $TRN_C \rightarrow TC_C$, which stood to interfere directly with TC_C's reception of a propagating signal, associated with the largest NRC of these three synapses (-0.207; Table 5).

A second-order regression model (R^2=0.857, RMSE=0.051, p<0.0001) disclosed a large, propagation-enhancing interaction between the two laterally inhibitory synapses (NRC=0.753), underscoring the same dependence of propagation on strong open-loop TC-TRN-TC connectivity as seen in homogeneously synaptic networks, but additionally demonstrating that propagation scores increased nonlinearly as a function of simultaneously increasing the weights of $TRN_A \rightarrow TC_B$ and $TRN_B \rightarrow TC_C$. Quadratic terms elucidated by this model confirmed that nearly all of the synapses highlighted in the linear regression analysis retained the same qualitative effects on propagation over the domain of their weights, despite the magnitudes of those effects changing as a function of synaptic weight (Table 5); one exception to this was $TRN_C \rightarrow TRN_B$, whose individual influence on propagation became negligibly positive at 450 nS. Interactions between TRN-TRN synapses of either variety and TRN-TC synapses tended diminish propagation, as did those between recurrent and lateral inhibitory TRN-TC synapses. Taken together, the linear and 2° regression models indicated that heterogeneous network permutations with strong laterally inhibitory TRN-TC synapses tended to best support propagation. We speculate that those synapses tending to diminish propagation, albeit all to a relatively small degree, shared in common the capacity to interfere with the precise spike timing required to propagate a signal continuously along the open-loop TC-TRN-TC subnetwork from $L4_A$ to $L4_C$: in some cases, this interference would arise due to uncorrelated TRN-mediated inhibition of TC neurons (polysynaptically in the cases of TRN_A=TRN_B and TRN_A=TRN_c and monosynaptically for $TRN_A \rightarrow TC_A$, $TRN_B \rightarrow TC_B$, and $TRN_C \rightarrow TC_C$) or in the case of $TRN_C \rightarrow TRN_A$ and $TRN_C \rightarrow TRN_B$, by disrupting the requisite TRN-driven PIR in the TC neurons.

607 Consistent response propagation across the length of the network was epitomized by Network a'
608 (propagation score=0.868), in which $TRN_A \rightarrow TC_B$ and $TRN_B \rightarrow TC_C$ were both relatively strong and those
609 synapses impeding propagation relatively weak (Fig. 6C, left).
610
611 Across the heterogeneously synaptic network permutations generated and analyzed, the mean oscillation
612 score was 0.438 ± 0.001, with scores ranging between 4×10^{-4} and 1; there was a very small negative
613 correlation between the propagation and oscillation scores of these networks (r=-0.0296, p=0.0008).
614 Although neither a linear (R^2=0.253, RMSE=0.131, p<0.0001) nor a second-order (R^2=0.388,
615 RMSE=0.118, p<0.0001) regression model accounted for a majority of the variability in oscillation scores
616 across surveyed heterogeneous networks, each analysis nevertheless illuminated different aspects of this
617 property's synaptic substrates. Linear regression analysis demonstrated that oscillation scores scaled
618 positively with all three recurrently inhibitory TRN-TC synapses (Fig. 6B), mirroring the dependence of
619 this network property on strong, global closed-loop TC-TRN-TC connectivity in homogeneously synaptic
620 network variants. That the most downstream of these synapses, $TRN_C \rightarrow TC_C$, was strongly correlated with
621 oscillation, with an NRC=1.000, corroborated the inferred role played by this synapse in generating what
622 was the dominant mode of oscillation for homogeneous networks. Network b' (oscillation score, 0.508)
623 was representative of a heterogeneous network variant in which this mechanism of oscillation was
624 prevalent (Fig. 6C, middle). Two intrareticular synapses, TRN_A-TRN_C and TRN_A=TRN_C, tended to
625 contribute modestly to oscillation (NRCs of 0.115 and 0.117, respectively), apparently representing
626 alternate though nondominant pathways through which oscillatory activity might propagate from one end
627 of the network to the other or be directly induced through successive bouts of PIR-mediated excitation in
628 TC_C via TRN_C (see Fig. 1B, left and middle pathways). By contrast, the two laterally inhibitory
629 reticulothalamic synapses, $TRN_A \rightarrow TC_B$ and $TRN_B \rightarrow TC_C$, tended to impede oscillation (NRCs of -0.289
630 and -0.379, respectively).
631

Although a 2° regression analysis confirmed that $TRN_A \rightarrow TC_B$ and $TRN_B \rightarrow TC_C$ were, in their individual capacities, strongly anticorrelated with oscillation in heterogeneous networks (NRCs of -1.000 and -0.892, respectively), interaction terms in this model involving these two synapses and any of the three recurrently inhibitory TRN-TC synapses ($TRN_A \rightarrow TC_A$, $TRN_B \rightarrow TC_B$, $TRN_C \rightarrow TC_C$) were moderately to strongly positive, with NRCs ranging between 0.345 and 0.669 (Table 5). Furthermore, in network permutations in which there was a continuum of strongly closed- and open-loop TC-TRN-TC motifs (i.e., networks in which both varieties of TRN-TC synapse were strongly expressed, allowing oscillatory activity to propagate reliably towards $TC_C/L4_C$), the cumulative oscillation-facilitating effects of these synaptic interactions superseded the attenuating, noninteractive effects of $TRN_A \rightarrow TC_B$ and $TRN_B \rightarrow TC_C$. Indeed, some such heterogeneous networks, as typified by Network c' (oscillation score, 1.000; Fig. 6C, right), supported degrees of oscillation that exceeded those of top-performing homogeneous networks, whose synaptic uniformity precluded architectures in which both recurrently and laterally inhibitory TRN-TC synapses were maximally weighted. Other interactions, such as those between $TRN_A \rightarrow TC_A$ and several intrareticular synapses, modestly hindered oscillation, apparently by diminishing the probability of periodically induced PIR in TC_A via TRN_A underlying oscillation in the former cell and the subsequent downstream propagation of this oscillatory activity; this interference could arise either from aperiodic inhibition of TRN_A ($TRN_B \rightarrow TRN_A$ x $TRN_A \rightarrow TC_A$, NRC=-0.186; $TRN_C \rightarrow TRN_A$ x $TRN_A \rightarrow TC_A$, NRC=-0.172) or through delaying/accelerating its spiking threshold via electrical coupling (TRN_A=TRN_C x $TRN_A \rightarrow TC_A$, NRC=-0.114). Although there were fewer heterogeneous network variants simulated (or theoretically possible) that possessed a synaptic architecture capable of supporting the propagation of oscillation than networks in which oscillation was borne of PIR-mediated oscillation via $TRN_C \rightarrow TC_C$, the former mode of oscillation was more strongly correlated with high oscillation scores among these networks, the opposite of what was observed in homogeneous networks: this was evidenced by the relative magnitudes of the second-order regression NRC of $TRN_C \rightarrow TC_C$ (0.107) and those of the synaptic interactions mediating propagation of oscillation.

Comparisons of network properties across synaptic architecture and external stimulation groups

We analyzed the relative capacities of homogeneously synaptic networks, whether stimulated externally in a fixed, punctate or sustained manner, and heterogeneous synaptic networks (for which TC_A was stimulated in a fixed, sustained manner) to support propagation and oscillation by comparing the 20 highest scores achieved by homogeneous and heterogeneous network permutations with respect to each performance metric. We decided against performing a direct comparison of mean performance scores across the full sets of homogeneous network permutations and surveyed heterogeneous network variants due to both unequal sample sizes (770 homogeneous vs. ~12,600 heterogeneous network permutations) and incomplete sampling of the full heterogeneous synaptic parameter space (less than 0.001% of all possible heterogeneously synaptic network variants were simulated in this study). As these caveats did not apply to the homogeneous networks alone, we were nevertheless able to employ repeated-measures comparisons of propagation and oscillation scores across the full set of 770 homogeneous network variants as a function of fixed stimulation condition (punctate vs. sustained) to more directly gauge the effect of different external stimulation durations on these network properties (see the *Response of homogeneously synaptic models to a fixed, sustained stimulus* subsection).

A one-way ANOVA disclosed no significant differences in mean propagation scores between top-performing network permutations across any of the three synaptic/stimulation groups [$F(2,57)=0.84$, $p=0.437$; Fig. 7]. We attributed this to the fact that synaptic regression analyses of both homogenously and heterogeneously networks, regardless of the fixed, eternal stimulation condition imposed on the former, predicted that similarly constituted homogeneous and heterogeneous network variants, namely those with 1) fully open-loop TC-TRN-TC architectures (equivalently, those in which $TRN_A \rightarrow TC_B$ and $TRN_B \rightarrow TC_C$ were maximally weighted) and 2) nonexistent intrareticular and recurrently inhibitory TRN-TC synapses, would rank among the top signal propagators. In contrast to propagation, the top scorers among heterogeneous network variants better supported oscillation than the top homogeneous performers, regardless of fixed stimulation condition [one-way ANOVA, $F(2,57)=166.14$, $p<0.0001$]. Pairwise mean oscillation differences assessed through Tukey's tests between top-performing heterogeneous networks and both groups of homogeneous networks were highly significant ($p<0.0001$), while there was no

686 significant difference in top homogeneous oscillation scores as a function of differing fixed, external
687 stimulation (p=0.153). We concluded that heterogeneously synaptic networks' superior capacity to
688 oscillate was most closely related to their greater relative ability to propagate oscillatory activity across
689 TC-TRN-L4 columns; as related in the preceding section, this mode of oscillation, when available,
690 yielded appreciably higher fidelity of oscillation than afforded by the effect of PIR-driven oscillation in
691 TC_C, itself predominant in homogeneous networks.
692
693 **Discussion:**
694 The data generated and analyzed in the present study confirmed our central hypothesis, that open-loop
695 TC-TRN-TC synaptic motifs (Fig. 1B, right) could function as a substrate for signal propagation within
696 the thalamus. Propagation scores were more strongly dependent on the more downstream of the two
697 laterally inhibitory reticulothalamic synapses, $TRN_B \rightarrow TC_C$, in heterogeneously synaptic networks. By
698 contrast, not only was propagation poorly supported through intrareticular synapses, both chemical or
699 electrical (Fig. 1B, left and middle, respectively), these pathways in fact generally interfered with the
700 spike timing underlying propagation across the TC-TRN subnetwork; for the same reason, recurrently
701 inhibitory TRN-TC synapses, which served no role in mediating signal propagation, also tended to
702 diminish networks' capacity to support this property. Changing the duration of the generalized external
703 stimulus delivered to networks from punctate (50 ms) to sustained (1,100 ms) did not significantly affect
704 propagation scores across the set of homogeneously synaptic network permutations, nor were there
705 differences observed between homogeneous and heterogeneous networks accommodating high degrees of
706 propagation.
707
708 Oscillation in model networks typically arose through one of two mechanisms: the first, which was both
709 more prevalent and strongly correlated with oscillation scores in homogeneous networks, relied on TRN_C-
710 mediated post-inhibitory rebound in TC_C that recurred at periodic intervals and could be sustained over
711 several hundred milliseconds. As such, this mode of oscillation was observed in networks exhibiting a
712 strongly weighted $TRN_C \rightarrow TC_C$ synapse, whether individually, as in heterogeneous network variants, or as

part of homogeneous networks with a uniformly strong closed-loop TC-TRN-TC architecture. This mechanism could be elicited either indirectly through stimulation of the network upstream of TC_C, including as a consequence of the fixed, external stimulus delivered to TC_A, or directly through spontaneous external stimulation of the former neuron. Comparatively more robust oscillation, persisting over a greater number of cycles and consequently associated with higher oscillation scores, was observed as a result of the other mode of oscillation, which entailed the propagation of oscillatory activity, as induced through sustained stimulation of TC_A, through a network. This oscillation mechanism was most likely to occur in networks exhibiting simultaneously strong closed- and open-loop TC-TRN-TC motifs and was therefore more prevalent in heterogeneous network permutations, where it was moreover more strongly determinative of oscillation scores than the other mode of oscillation. For this reason, the mean oscillation score of top-performing heterogeneous networks was significantly higher than those of their homogeneous counterparts; (across the full set of homogeneously synaptic networks, fixed, sustained stimulation slightly enhanced oscillation scores over those attained through punctate stimulation). Synaptic interactions that impeded the latter mode of oscillation typically interfered with the induction of oscillatory activity through PIR in $TRN_A \rightarrow TC_A$ by disrupting the temporal dynamics of this process and precluding this activity from propagating downstream. A third, relatively weak and infrequently observed form of oscillation also involved oscillatory activity propagating from one end of the network to the other by way of TRN_A-TRN_C and TRN_A=TRN_C.

Methodological considerations of the study

In an effort to maximize the predictive potential of our neural model relative to computational demands that can increase exponentially with increasing degrees of freedom, we relied in some instances on simplifications and/or idealizations, while in other cases, deliberately omitted experimentally verified biophysical and neurophysiological details of the thalamo-reticulo-cortical networks being simulated and their individual neuronal constituents. Such details can, in principle, can be selectively added to future iterations of this model to explore questions and phenomena related to those posed and examined in the present study.

Two points should be made regarding the constitution of the model neurons used in our study. First, like most of the thalamic (Destexhe et al., 1993; Destexhe et al., 1994; Golomb et al., 1996; Destexhe et al., 1996a; Sohal and Huguenard, 1998; Bazhenov et al., 1998) and thalamocortical models (Destexhe et al., 1998; Bazhenov et al., 2002; Rogala et al., 2013) that inspired our model, we utilized single-compartment, Hodgkin-Huxley neurons. While these model cells contribute to the computational parsimony and practicality of network models, particularly where the analysis of network dynamics is prioritized, they neglect the intrinsic cable properties of real neurons and, relatedly, the spatially disparate nature of synaptic integration and heterogeneous expression of intrinsic and synaptic conductances (Dayan and Abbott, 2005; Herz et al., 2006). Such considerations are particularly relevant here relative to dendritic distributions of t- current and h-current in TC neurons (McCormick and Pape, 1990; Destexhe et al., 1998; Williams and Stuart, 2000; Traub et al., 2005) and TRN neurons (Contreras et al., 1993; Destexhe et al., 1996b; Traub et al., 2005; Crandall et al., 2010). Multicompartment neuronal models incorporating such details could conceivably alter the network dynamics being studied. Second, although we allowed for heterogeneous connections within a given synaptic class for a subset of simulated network permutations, all cells within each of the three network layers were modeled with identical intrinsic parameters. In reality, even anatomically proximal populations of TC, TRN, and layer 4 cortical neurons each exhibit a wide spectrum of different intrinsic properties (Leresche et al., 1991; Spreafico et al., 1991; Lee et al., 2007; Landau et al., 2016), with the variability of these neurons' synaptic "footprints" in space often well exceeding what we capture in our model (Cox et al., 1996; Cox et al., 1997; Pinault et al., 1997). If larger-scale elaborations of the model are simulated in the future, both the cellular and spatial synaptic variability observed experimentally could be approximated by allowing given parameters to vary systematically or at random within physiological ranges, much as we did with TRN-TRN and TRN-TC synaptic conductances in the present study; this would allow any such model to approach a more representative degree of anatomical and functional heterogeneity.

In the interest of isolating the feedforward dynamics of thalamocortical transmission intrinsic to our present model, certain synaptic connections to TC, TRN, and L4 neurons were either excluded or generalized. First, while Poisson processes are often utilized to represent complex, noisy, and/or generalized synaptic inputs (Dayan and Abbott, 2005), it is reasonable, given the coherence of activity across anatomically disparate regions of the brain that prevails during sensory processing, that canonically non-sensory brain regions projecting to the both the TRN and dorsal thalamus might exhibit activity correlated with ascending sensory input, making the use of stochastic inputs to TC neurons of our model a crucially simplifying but imprecise approximation. Similarly, although the high-frequency pulse trains we employed as generalized external stimuli within the model belie the rich and variable stimulus encoding schemes inherent to different sensory systems, these rudimentary stimulus approximations, in combination with the baseline stochastic input, were nevertheless sufficient to elicit propagating and/or oscillating waves in the model network and analyze their dynamics across network permutations, reflecting the use of similar pulse trains to generate spindle-like waves in isolated thalamic slices and analysis of how those waves were perturbed as a function of various pharmacological manipulations (Bal et al., 1995; Kim et al., 1995). Although we chose not to emphasize the correlation between stimulus and response in the present study, in keeping with similar thalamo-reticulo(-cortical) modeling studies (e.g., Destexhe et al., 1996a, Golomb et al., 1996; Sohal and Huguenard, 1998; Bazhenov et al., 1998, Traub et al., 2005), future efforts using the present baseline network model or elaborations thereof might investigate response dynamics as a function of varying spatial and/or temporal stimulus profiles (see, for example, Pham and Haas, 2018). A more realistic rendering of stimulus representations in this modeling paradigm might also account for the subset of inhibitory afferents projecting to parts of the thalamus, including the lateral geniculate nuclei and medial geniculate bodies (Cucchiaro et al., 1991; Winer et al, 1996; Peruzzi et al., 1997; Llano et al., 2014).

Additionally, the present model omitted explicit corticothalamic and corticoreticular synapses, both of which have been identified and physiologically characterized to varying degrees (Steriade et al., 1972; White and Hersch, 1982; DeCurtis et al., 1989; Contreras et al., 1996; Blumenfeld and McCormick, 2000;

Zhang and Jones, 2004; Crandall et al., 2015), though the former were effectively amalgamated with both feedforward sensory and modulatory projections to the thalamus in the form of the generalized, Poisson-modulated external input we delivered to individual TC neurons. Both forms of feedback have been implicated in the spread of spindle waves and in the maintenance of their synchronization over large distance scales (on the order of the length of the mammalian forebrain) and are furthermore known to drive spindle wave formation *in vivo* by polysynaptically recruiting TC neurons via TRN-mediated PIR (Steriade et al., 1972; Roy et al., 1984; Contreras and Steriade, 1996; Contreras et al., 1996; Suga and Ma, 2003; Sillito et al., 2006; Crandall et al., 2015). It should be noted, however, that short-range coherence of spindle waves, which can be elicited in isolated thalamic slice preparations (Bal et al., 1995; Kim et al., 1995), is preserved following decortication, both *in vivo* and *in silico* (Contreras and Steriade, 1996; Contreras et al., 1996; Destexhe et al., 1998). By extension, it is reasonable to assume that the dynamics of the spindle-like waveforms generated in our small-scale, broadly feedforward model, in which the cortex served solely as an output layer, would not be qualitatively altered by corticothalamic or corticoreticular feedback. An additional challenge in modeling descending cortical projections lies in rendering the complex intracolumnar interactions between multiple cortical layers upstream of them: several thalamocortical models incorporating corticothalamic and corticoreticular feedback limited cortical representation to layer 6 neurons and/or fast-spiking interneurons (Destexhe et al., 1998; Bazhenov et al., 2002; Rogala et al., 2013), while Traub et al. (2005) simulated six distinct cortical populations within layers 2-6 as part of an expansive thalamocortical network model comprising 3,560 multicompartment neurons. Future efforts within our modeling paradigm stand to both expand the spatial scale of the thalamocortical network and incorporate reciprocal cortical projections involving interactions between multiple cortical layers.

Finally, external inputs to the TRN were also omitted from the model. Although it is recognized that the TRN receives a variety of inputs from beyond the thalamus and sensory cortex (Asanuma and Porter, 1990; Bickford et al., 1994; Zikopoulos and Barbas, 2006; Sun et al., 2013; Pita-Almenar et al., 2014), an early version of our model that included stochastic external inputs to TRN neurons mirroring those

delivered to the TC layer did not significantly alter network dynamics beyond marginally increasing variability in those network properties studied.

Comparison to related computational models and physiological data

Although the production of spindle waves was not an explicit objective of our study, some of the wave dynamics arising in our networks were nevertheless consistent with those inherent to spindle or spindle-like waves, as observed empirically or generated in other modeling studies. Despite possessing higher degrees of TC→TRN and TRN→TC synaptic divergence and lacking the exclusively open-loop TC-TRN-TC architecture characterizing a subset of our network variants, other isolated thalamic models allowing for longitudinal wave propagation similarly accommodated this propagation along the lattice of interconnected TC and TRN neurons by way of laterally inhibitory TRN-TC synapses (Kim et al., 1995; Destexhe et al., 1996a; Golomb et al., 1996; Bazhenov et al., 1998; Muller and Destexhe, 2012); at short ranges, this mechanism of signal propagation also prevailed in large-scale thalamo-reticulo-cortical models, while corticothalamics acted to propagate activity to more distal sites (Destexhe et al., 1998; see Destexhe and Sejnowski, 2003, for a schematic illustrating short- and long-range thalamocortical wave propagation). Comparably, recurrently inhibitory TRN-TC synapses have been documented to play a vital role in the generation of oscillatory behavior in the thalamus (Steriade and Deschênes, 1984; von Krosigk et al., 1993). The temporal parameters of propagating and oscillation signals in our model also matched some of those previously reported: among homogeneously synaptic network permutations, the mean velocity of signal propagation across the length of the network was approximately 0.50 mm/s, which was consistent with the propagation velocity of spindle waves measured in a ferret thalamic slice and about half as fast as values reported in computational models of this slice preparation (Kim et al., 1995; Golomb et al., 1996; Destexhe et al., 1996a). Similarly, the roughly 9.1-Hz mean oscillation frequency measured across homogeneous networks fell within the 6-12 Hz range of intraspindle spike frequencies reported in both physiological and computational spindle wave studies (Andersen and Andersson, 1968; Steriade and Deschênes, 1984; Kim et al., 1995; Golomb et al., 1996; Destexhe et al., 1996a).

847 Several key structural elements of our set of network models and the range of phenomenology they
848 produced distinguish them from previous thalamic and thalamocortical models. One particularly notable
849 point of departure relative to similar network models was the extent to which thalamoreticular,
850 reticulothalamic, and thalamocortical synapses diverged. Although all three classes of synapses are
851 known to diverge significantly and have been observed to target neuronal somata hundreds of microns
852 from their origins (Jones, 1985; Crabtree, 1996; Cox et al., 1996; Cox et al., 1997; Pinault and Deschênes,
853 1998; Sherman and Guillery, 2001; Alonso et al., 2001; Miller et al., 2001), the TC-TRN, TRN-TC, and
854 TC-L4 synapses in our model were constrained to remain strictly local and minimally divergent (or non-
855 divergent, in the case of TC-TRN and TC-L4 synapses). With respect to the first two classes of synapses,
856 this constraint was imposed in order to preserve the disynaptic TC-TRN-TC open-loop motifs
857 characterizing a subset of network permutations, which constituted one of the focuses of our study, and
858 analyze the signal propagation they may support. This neuroanatomical scheme contrasted with previous
859 computational models featuring parallel, interconnected thalamoreticular pathways, in which both TC and
860 TRN synapsed bidirectionally with several neighboring TRN and TC cells, respectively, within a radius
861 of several hundred microns (e.g., Golomb et al., 1996; Destexhe et al., 1996a; Destexhe et al., 1998; Sohal
862 and Huguenard, 1998; Sohal et al., 2000; Bazhenov et al., 1998; Bazhenov et al., 2002; Traub et al., 2005;
863 Izhikevich and Edelman, 2008).
864
865 The contrasting synaptic architectures between our network model and other isolated thalamic models
866 accounted for several important differences in the waveforms documented in this study and those
867 previously observed *in simulo*. First, the asymmetric distribution of the laterally inhibitory TRN-TC
868 synapses in our model generally restricted the propagation of signals to a single direction, whereas
869 bidirectional wave propagation was observed in several other network models marked by greater degrees
870 TC-TRN and TRN-TC synaptic divergence when these networks were externally stimulated in their
871 anatomical centers (Bazhenov et al., 1998; Sohal et al., 2000). Relatedly, whereas some percentage of the
872 stimulus-driven responses and spontaneous signals arising in Column A of our network tended to
873 dissipate before arriving at Column C due to either spike failure or extraneous network activity interfering

with the temporal dynamics required for uninterupted propagation (see, for example, Fig. 3, in which spikes associated with a single epoch of propagation that were tallied across simulations of the same network diminished between $L4_A$ and $L4_C$), the presence of bidirectional, divergent thalamoreticular and reticulothalamic synapses in other network models were associated with less dampened, longer-duration, and in larger networks, longer-distance signal propagation, a property ostensibly attributable to the greater interconnectedness between TC and TRN neurons throughout these networks and a resulting degeneracy of signaling pathways (Destexhe et al., 1996a; Golomb et al., 1996; Bazhenov et al., 1998; Sohal and Huguenard, 1998).

We emphasize, however, that the discrepancy in spatiotemporal signal coherence between our network model and others was also likely a function of disparate network inputs: on the one hand, fixed external input was applied periodically to certain networks (Destexhe et al., 1996a; Bazhenov et al., 1998; Rinzel et al., 1998), rather than over a singular interval as in ours, or distributed over multiple neurons in a spatially dependent manner (Bazhenov et al., 1998; Sohal et al., 2000; Pham and Haas, 2018), in contrast to the application of fixed stimulation to a single neuron (in our model, TC_A). Arguably more integral to the difference in signal integrity was the stochastic input received by neurons in the TC layer of our model network: as detailed in our analysis, these inputs elicited sufficient noise to interfere intermittently with efficient propagation and oscillation. Other thalamic and thalamocortical model networks lacked these inputs, and indeed some remained fully quiescent in the absence of external stimulation (Destexhe et al., 1993; Golomb et al., 1996; Rinzel et al., 1998; Bazhenov et al., 1998; Sohal et al., 2000; Traub et al., 2005). We moreover ascribe the absence of the “waxing and waning” patterns of activation lasting 0.5-2 s in TC, TRN, and cortical cell populations that characterize spindle waves, as measured experimentally in individual TC and TRN neurons (Steriade and Llinàs, 1988; Leresche et al., 1991; Soltesz et al., 1991; von Krosigk et al., 1993), observed across neuronal population through electroencephalography and local field potential recordings (Gibbs and Gibbs, 1950; Andersen and Andersson, 1968; Steriade and Deschênes, 1984; Steriade et al., 1987), and generated in network models aimed at reproducing the spindling phenomenon (Destexhe et al., 1993; Destexhe et al., 1994; Destexhe et

al., 1996a; Bazhenov et al. 1999), to the presence of stochastic activity in our model. Although the thalamic relay neurons in our model expressed the h-current and, in a subset of network permutations, the reciprocal TC-TRN connections thought to account for spindling, the phenomenon also presupposes a sustained antiphase relationship between TC and TRN spiking over the course of an individual spindle wave that was invariably disrupted by the stochastic input to our network (Destexhe et al., 1993; Bal and McCormick, 1996; Luthi and McCormick, 1998; Timofeev et al., 2001). That spindle waves still occur *in vivo* during sleep despite a myriad of inputs impinging on the dorsal thalamus and TRN that would tend to perturb the intrinsic and synaptic conductances underlying the waveform suggests a countervailing source of spindle maintenance: this role could conceivably be filled by corticothalamics, which have been demonstrated to synchronize spindle-wave activity over large distances in the brain (Bal et al., 1995; Contreras and Steriade, 1996; Timofeev et al., 2001; Bonjean et al., 2011).

We finally wish to comment on the finding that intrareticular synapses, both GABAergic and electrical, manifested relatively little effect on the signal propagation and oscillation we observed in this study, despite having been copiously studied, simulated, and demonstrated to modulate certain waveforms arising in both the isolated thalamus and broader thalamocortical system (Ahlsén and Lindström, 1982; Steriade et al., 1990; Sanchez-Vives et al., 1997; Sohal et al., 2000; Landisman et al., 2002; Long et al., 2004; Fuentealba et al., 2004; Deleuze and Huguenard, 2006; Lam et al., 2006). To the extent that GABAergic intrareticular synapses disrupted efficient signal propagation along the length of our networks, this could conceivably lend credence to the contention of Deleuze and Huguenard (2006), who, based on their observation that TRN-TRN$_{GABA}$ synapses were more densely distributed along the dorsoventral (vertical) axis of the TRN, posited that these synapses may selectively filter sensory input as it traverses the thalamus to reach the cortex and play a less consequential role with respect to horizontal (intrathalamic) signal propagation. Notwithstanding the potentially paradigm-shifting question as to whether TRN-TRN$_{GABA}$ synapses are altogether absent in certain mammals or degenerate as a function of increasing age (Landisman et al., 2002; Cruikshank et al., 2010; Hou et al., 2016), it has moreover been shown in thalamic slice preparations derived from juvenile rodents, with supporting computational

models, that pharmacologically blocking or knocking out the expression of intrareticular GABAergic synapses promotes large-scale synchronization of ~3-Hz spike-wave discharges in the thalamus that resemble absence seizures; TRN-TRN$_{GABA}$ synapses are thus thought to desynchronize activity in a way that preserves normal thalamic function while staving off epileptiform patterns in affected animals (von Krosigk et al., 1993; Bal et al., 1995; Huntsman et al., 1999; Sohal et al., 2000; Sohal and Huguenard, 2003; Traub et al., 2005). Although intrareticular synapses were shown in the present study to modestly dampen propagation through open-loop TC-TRN-TC architectures, both the relative lack of synaptic divergence, as discussed above, and the limited scale of our model network would have likely precluded any meaningful observations of neuronal synchrony or lack thereof as a function of TRN-TRN$_{GABA}$ weighting. It should additionally be stated that reticulothalamic signaling mediated through GABA$_B$ receptors is thought to contribute to the sustained hyperpolarization of thalamic relay neurons observed in absence-like waveforms, and these receptors were not included in our model (von Krosigk et al., 1993; Bal et al., 1995; Pinault et al., 1998; Crunelli and Leresche, 2002; Sohal and Huguenard, 2003).

As was the case with chemical synapses in the TRN, TRN-TRN$_{Elec}$ synapses did not mediate signal propagation and supported comparatively weak forms of oscillation in a minority of network permutations. With respect to the former property, our results were consistent with predictions that follow from two sets of physiological observations made on these synapses: 1) across three separate studies, electrical postsynaptic potentials or "spikelets," from which electrical coupling can be inferred, were observed in less than 50% of observed TRN neuron pairs [Landisman et al., 2002; Deleuze and Huguenard, 2006; Lam et al., 2006; Lee et al., 2014; note that Long et al. (2004) reported this figure at 71% but speculated that the discrepancy owed to recording from cell pairs with <5 μm edge-edge separation]; and 2) mean electrical coupling coefficients between TRN neurons were small [0.032, as reported by Landisman et al. (2002); ~0.02, Fuentealba et al. (2004); 0.11, as measured in closely apposed cells by Long et al. (2004)]. These data suggest that 1) TRN-TRN$_{Elec}$ synapses are too sparsely distributed to facilitate uninterrupted signal propagation within the TRN over large scales and 2) electrical coupling between TRN neurons, even between those extremely closely situated to one another, is typically

insufficient to allow action potentials in one neuron to induce concurrent action potentials in its coupled partner. Indeed, we only observed direct electrical induction of action potentials in those network permutations exhibiting the highest degree of electrical coupling [0.36, close to the maximum coupling strength observed by Landisman et al. (2002) and Long et al. (2004); see the middle panel of Fig. 4C for an example of this phenomenon]. Nevertheless, gap junctions found between TRN neurons have been demonstrated to play important roles vis-à-vis thalamic signaling: in keeping with their ability to act as low-pass filters, TRN-TRN$_{Elec}$ synapses have been documented to promote thalamocortical synchronization of subthreshold activity and low-frequency oscillations (<10 Hz), including components of spindle waves (Long et al., 2004; Fuentealba et al., 2004; Traub et al., 2005), and can conceivably facilitate the temporal discrimination of multiple near-coincident sensory stimuli by the cortex (Pham and Haas, 2018). Furthermore, it has been suggested, based on the recent discovery of activity-dependent plasticity of electrical coupling strength in brain regions including the TRN (Haas et al., 2011; Haas and Landisman, 2012; Wang et al., 2015; Kohmann et al., 2016), that gap junction plasticity in the TRN might itself underlie the generation of spindle waves (Pernelle et al., 2017). It remains an outstanding question and one easily amenable to future investigation through computational modeling whether open-loop TC-TRN-TC architectures, either independently of or in cooperation with intrareticular synapses, modulate neuronal synchrony.

The function and scale of open-loop thalamo-reticulo-thalamic synaptic motifs

It is essential to contextualize the predictive potential of our model and the broader functions conceivably served by open-loop TC-TRN-TC architectures. As discussed, the networks designed for this study did not and were not intended to produce the gamut of phenomenology documented in the thalamocortical system. Rather, they function as idealized network modules that could hypothetically exist within surrounding neuronal populations. Open-loop TC-TRN-TC configurations have thus far been observed both within and across individual thalamic nuclei (both first- and higher-order) and are thought to serve as pathways for intra- and cross-modal modulation, respectively (Crabtree et al., 1998; Pinault and Deschênes, 1998; Crabtree and Isaac, 2002; Lam and Sherman, 2005; Lee et al., 2010; Kimura et al.,

2007; Kimura, 2014; Lam and Sherman, 2015). However, despite available data on the distances over which TRN neurons may project to synapse with TC cells (Cox et al., 1996), the proportion of recurrently to laterally inhibitory TRN-TC synapses in any thalamic nucleus and the spatial homogeneity of these connections remain unknown, and thus the density and distribution of open-loop TC-TRN-TC architectures are questions as yet unanswered; the full extent of open-loop connections between thalamic nuclei is similarly indeterminate. As such, our small network model could be easily rescaled to approximate the physiological dimensions of these connections as such information becomes available, adjusting synaptic delays accordingly.

Although the anatomical bases of open-loop TC-TRN-TC motifs have been partially characterized, their functional significance in the brain lingers as a subject of continued speculation. As has been previously surmised, these synaptic pathways could plausibly lend themselves to sensory enhancement, multisensory integration, and attentional mechanisms (Crabtree and Isaac, 2002; Pinault, 2004; Willis et al., 2015; Crabtree, 2018). Whereas a full elucidation of such phenomena vis-à-vis thalamoreticular connectivity lies well beyond the scope of this study and will likely depend upon a far more nuanced understanding of how perceptual processes are born out of interplay between the cortex, dorsal thalamus, TRN, and likely other brain structures, our model can nevertheless offer more fundamental predictions about the capacity of open-loop TC-TRN-TC configurations to accommodate basic signaling properties within the thalamus. First, as inferred from physiological studies, open-loop pathways should be fully capable of supporting signaling propagation from one thalamic relay neuron to another through a limited number of intervening synapses (with a disynaptic pathway serving as the shortest such configuration), whether or not the target neuron lies in the same thalamic nucleus. Secondly, a localized thalamic region consisting exclusively of interconnected open-loop TC-TRN-TC motifs (homogeneously synaptic) or a sequence of spatially separated, interconnected laterally inhibitory TRN-TC synapses, should either exist, might be capable of supporting a non-periodic signal (e.g., a transient sensory-evoked signal) propagating between multiple thalamic relay neurons, subject to the nature of the signal, the input(s) generating it, and potentially limited by the degree of spontaneous (decohering) activity along the

signaling pathway. It is unclear how the fidelity of a transient signal in either scenario would compare to that measured along a more densely interconnected segment of thalamus characterized by greater thalamoreticular and reticulothalamic divergence, as traditionally conceived of in earlier modeling studies (Destexhe et al., 1996a; Golomb et al., 1996; Bazhenov et al., 1998) and in which a signal might feed back on itself; this is despite the fact that the latter architectures are capable of accommodating sustained, periodic waveforms such as sleep spindles. Thirdly, discrete thalamic regions marked by synaptic heterogeneity should be equally capable of propagating signals as those characterized by TC-TRN and TRN-TC synaptic uniformity, after accounting for differences in the average weights or spatial densities of laterally inhibitory TRN-TC synapses. Indeed, if the morphological, intrinsic, and synaptic heterogeneity of TRN neurons are any indication (Schiebel and Schiebel, 1966; Jones, 1975; Spreafico et al., 1988; Spreafico et al., 1991; Cox et al., 1996; Brunton and Charpak, 1997; Lee et al., 2007; Bickford, 2016), it is reasonable to assume that both thalamorectiular and reticulothalamic synapses are typically distributed in a heterogeneous manner across the thalamus. Lastly, unless driven by an external oscillatory source, whether ascending or descending, oscillatory waveforms should not subsist in a localized thalamic region populated exclusively by open-loop connections. Both forthcoming physiological investigation and future modeling studies will undoubtedly be able to evaluate some of these predictions.

Acknowledgments:

This work made use of the Illinois Campus Cluster, a computing resource that is operated by the Illinois Campus Cluster Program (ICCP) in conjunction with the National Center for Supercomputing Applications (NCSA) and which is supported by funds from the University of Illinois at Urbana-Champaign. We additionally thank Profs. Thomas Anastasio and Ruoqing Zhu, Drs. Rama Ratnam and Baher Ibrahim, and Mr. Weddie Jackson for their valuable analytical, statistical, and technical insights.

References:

1. Smith PH, Bartlett EL, Kowalkowski A (2006) Unique combination of anatomy and physiology in cells of the rat paralaminar thalamic nuclei adjacent to the medial geniculate body. *J Comp Neurol* 496(3):314-334.

2. Lee SC, Cruikshank SJ, Connors BW (2010) Electrical and chemical synapses between relay neurons in developing thalamus. *J Physiol* 588(13):2403-2415.

3. Guillery SW, Sherman SM (2002) Thalamic relay functions and their role in corticocortical communication: generalizations from the visual system. *Neuron* 33(2):163-175.

4. Sherman SM (2004) Interneurons and triadic circuitry of the thalamus. *Trends Neurosci* 27(11):670-675.

5. Pinault D (2004) The thalamic reticular nucleus: structure, function and concept. *Brain Res Brain Res Rev* 46(1):1-31.

6. Crick F (1984) Function of the thalamic reticular complex: the searchlight hypothesis. *Proc Natl Acad Sci USA* 81(14):4586-4590.

7. Guillery RW, Feig SL, Lozsádi DA (1998) Paying attention to the thalamic reticular nucleus. *Trends Neurosci* 21(1):28-32.

8. McAlonan K, Cavanaugh J, Wurtz RH (2006) Attentional modulation of thalamic reticular neurons. *J Neurosci* 26(16):4444-4450.

9. Llinás RR, Paré D (1991) Of dreaming and wakefulness. *Neuroscience* 44(3):521-535.

10. Steriade M, McCormick D, Sejnowski T (1993) Thalamocortical oscillations in the sleeping and aroused brain. *Science* 262(5134):679-685.

11. von Krosigk, M, Bal T, McCormick DA (1993) Cellular mechanisms of a synchronized oscillation in the thalamus. *Science* 261(5119):361-364.

12. Bal T, von Krosigk M, McCormick DA (1995) Role of the ferret perigeniculate nucleus in the generation of synchronized oscillations in vitro. *J Physiol* 483(3):665-685.

13. Destexhe A, Bal T, McCormick DA, Sejnowski TJ (1996) Ionic mechanisms underlying synchronized oscillations and propagating waves in a model of ferret thalamic slices. *J Neurophysiol* 76(3):2049-2070.

14. Huguenard JR (1998) Neuronal circuitry of thalamocortical epilepsy and mechanisms of antiabsence drug action. *Adv Neurol* 79:991-999.

15. McCormick DA, Contreras D (2001) On the cellular and network bases of epileptic seizures. *Annu Rev Physiol* 63:815-846.

16. Wells MF, Wimmer RD, Schmitt LI, Feng G, Halassa MM (2016) Thalamic reticular impairment underlies attention deficit in Ptchd1(Y/-) mice. *Nature* 532(7597):58-63.

17. Krol A, Wimmer RD, Halassa MM, Feng G (2018) Thalamic reticular dysfunction as a circuit endophenotype in neurodevelopmental disorders. *Neuron* 98(2):282-295.

18. Sherman SM, Guillery RW (2001) Exploring the thalamus (Academic Press, San Diego).

19. Steriade M, Deschênes M (1984) The thalamus as a neuronal oscillator. *Brain Res* 320(1):1-63.

20. Steriade M, Domich L, Oakson G, Deschênes M (1987) The deafferented reticular thalamic nucleus generates spindle rhythmicity. *J Neurophysiol* 57(1):260-273.

21. Kim U, Bal T, McCormick DA (1995) Spindle waves are propagating synchronized oscillations in the ferret LGNd in vitro. *J Neurophysiol* 74(3):1301-1323.

22. Ulrich D, Huguenard, JR (1997) GABA(A)-receptor-mediated rebound burst firing and burst shunting in thalamus. *J Neurophysiol* 78(3):1748-1751.

23. Hale PT, Sefton AJ, Bauer LA, Cottee LJ (1982) Interrelations of the rat's thalamic reticular and dorsal lateral geniculate nuclei. *Exp Brain Res* 45(1-2):217-229.

24. Warren RA, Agmon A, Jones EG (1994) Oscillatory synaptic interactions between ventroposterior and reticular neurons in mouse thalamus in vitro. *J Neurophysiol* 72(4):1993-2003.

25. Sherman SM, Guillery RW (1996) Functional organization of thalamocortical relays. *J Neurophysiol* 76(3):1367-1395.

26. Shosaku A (1986) Cross-correlation analysis of a recurrent inhibitory circuit in the rat thalamus. *J Neurophysiol* 55(5):1030-1043.

27. Lo FS, Sherman SM (1994) Feedback inhibition in the cat's lateral geniculate nucleus. *Exp Brain Res* 100(2):365-368.

28. Gentet LJ, Ulrich D (2003) Strong, reliable and precise synaptic connections between thalamic relay cells and neurones of the nucleus reticularis in juvenile rats. *J Physiol* 546(3):801-811.

29. Pinault D, Deschênes M (1998) Anatomical evidence for a mechanism of lateral inhibition in the rat thalamus. *Eur J Neurosci* 10(11):3462-3469.

30. FitzGibbon T, Solomon SG, Goodchild AK (2000) Distribution of calbindin, parvalbumin, and calretinin immunoreactivity in the reticular thalamic nucleus of the marmoset: evidence for a medial leaflet of incertal neurons. *Exp Neurol* 164(2):371-383.

31. Crabtree JW, Collingridge GL, Isaac JT (1998) A new intrathalamic pathway linking modality-related nuclei in the dorsal thalamus. *Nat Neurosci* 1(5):389-394.

32. Crabtree JW, Isaac JT (2002) New intrathalamic pathways allowing modality-related and cross-modality switching in the dorsal thalamus. *J Neurosci* 22(19):8754-8761.

33. Lam YW, Sherman SM (2005) Mapping by laser photostimulation of connections between the thalamic reticular and ventral posterior lateral nuclei in the rat. *J Neurophysiol* 94(4):2472–2483.

34. Lam YW, Sherman SM (2015) Functional topographic organization of the motor reticulothalamic pathway. *J Neurophysiol* 113(9):3090-3097.

35. Kimura A, Imbe H, Donishi T, Tamai Y (2007) Axonal projections of single auditory neurons in the thalamic reticular nucleus: implications for tonotopy-related gating function and cross-modal modulation. *Eur J Neurosci* 26(12):3524-3535.

36. Kimura A (2014) Diverse subthreshold cross-modal sensory interactions in the thalamic reticular nucleus: implications for new pathways of cross-modal attentional gating function. *Eur J Neurosci* 39(9):1405-1418.

37. Asanuma C, Porter LL (1990) Light and electron microscopic evidence for a GABAergic projection from the caudal basal forebrain to the thalamic reticular nucleus in rats. *J Comp Neurol* 302(1):159-172.

38. Bickford ME, Günlük AE, Van Horn SC, Sherman SM (1994) GABAergic projection from the basal forebrain to the visual sector of the thalamic reticular nucleus in the cat. *J Comp Neurol* 348(4):481-510.

39. Zikopoulos B, Barbas H (2006) Prefrontal projections to the thalamic reticular nucleus form a unique circuit for attentional mechanisms. *J Neurosci* 26(28):7348-7361.

40. Sun YG, Pita-Almenar JD, Wu CS, Renger JJ, Uebele VN, Lu HC, Beierlein M (2013) Biphasic cholinergic synaptic transmission controls action potential activity in thalamic reticular nucleus neurons. *J Neurosci* 33(5):2048–2059.

41. Pita-Almenar JD, Yu D, Lu HC, Beierlein M (2014) Mechanisms underlying desynchronization of cholinergic-evoked thalamic network activity. *J Neurosci* 34(43):14463–14474.

42. Destexhe A, McCormick DA, Sejnowski TJ (1993) A model for 8–10 Hz spindling in interconnected thalamic relay and reticularis neurons. *Biophys J* 65(6):2473–2477.

43. Destexhe A, Contreras D, Sejnowski TJ, Steriade M (1994) A model of spindle rhythmicity in the isolated thalamic reticular nucleus. *J Neurophysiol* 72(2):803–818.

44. Golomb D, Wang XJ, Rinzel J (1996) Propagation of spindle waves in a thalamic slice model. *J Neurophysiol* 75(2):750-769.

45. Sohal VS, Huguenard JR (1998) Long-Range Connections Synchronize Rather Than Spread Intrathalamic Oscillations: Computational Modeling and In Vitro Electrophysiology. *J Neurophysiol* 80(4):1736-1751.

46. Bazhenov M, Timofeev I, Steriade M, Sejnowski TJ (1998) Computational models of thalamocortical augmenting responses. *J Neurosci* 18(16):6444-6465.

47. Wasylenko TM, Cisternas JE, Laing CR, Kevrekidis IG (2010) Bifurcations of lurching waves in a thalamic neuronal network. *Biol Cybern* 103(6):447-62.

48. Pham T, Haas JS (2018) Electrical synapses between inhibitory neurons shape the responses of principal neurons to transient inputs in the thalamus: a modeling study. *Sci Rep* 8(1):7763.

49. Destexhe A, Contreras D, Steriade M (1998) Mechanisms underlying the synchronizing action of corticothalamic feedback through inhibition of thalamic relay cells. *J Neurophysiol* 79(2):999–1016.

50. Bazhenov M, Timofeev I, Steriade M, Sejnowski TJ (2002) Model of thalamocortical slow-wave sleep oscillations and transitions to activated states. *J Neurosci* 22(19):8691–8704.

51. Traub RD, Contreras D, Cunningham MO, Murray H, LeBeau FE, Roopun A, Bibbig A, Wilent WB, Higley MJ, Whittington MA (2005) Single-column thalamocortical network model exhibiting gamma oscillations, sleep spindles, and epileptogenic bursts. *J Neurophysiol* 93(4):2194-2232.

52. Izhikevich EM, Edelman GM (2008) Large-scale model of mammalian thalamocortical systems. *Proc Natl Acad Sci USA* 105(9):3593-8.

53. Rogala J, Waleszczyk WJ, Lęski S, Wróbel A, Wójcik DK (2013) Reciprocal inhibition and slow calcium decay in perigeniculate interneurons explain changes of spontaneous firing of thalamic cells caused by cortical inactivation. *J Comput Neurosci* 34(3):461-476.

54. Willis AM, Slater BJ, Gribkova ED, Llano DA (2015) Open-loop organization of thalamic reticular nucleus and dorsal thalamus: a computational model. *J Neurophysiol* 114(4):2353-2367.

55. Sherman SM (2001) Tonic and burst firing: dual modes of thalamocortical relay. *Trends Neurosci* 24(2):122–126.

56. Halassa MM, Siegle JH, Ritt JT, Ting JT, Feng G, Moore CI (2011) Selective optical drive of thalamic reticular nucleus generates thalamic bursts and cortical spindles. *Nat Neurosci* 14(9):1118–1120.

57. Ahlsén, G, Lindström, S (1982) Mutual inhibition between perigeniculate neurones. *Brain Res* 236(2):482-486.

58. Steriade M, Jones EG, Llinás RR (1990) Thalamic Oscillations and Signaling (Wiley-Interscience, New York).

59. Cox CL, Huguenard JR, Prince DA (1996) Heterogeneous axonal arborizations of rat thalamic reticular neurons in the ventrobasal nucleus. *J Comp Neuro* 366(3):416-430.

60. Sanchez-Vives, MV, Bal T, McCormick DA (1997) Inhibitory interactions between perigeniculate GABAergic neurons. *J Neurosci* 17(22):8894-8908.

61. Shu Y, McCormick DA (2002) Inhibitory interactions between ferret thalamic reticular neurons. *J Neurophysiol* 87(5):2571-2576.

62. Deleuze C, Huguenard (2006) Distinct electrical and chemical connectivity maps in the thalamic reticular nucleus: potential roles in synchronization and sensation. *J Neurosci* 26(33):8633-8645.

63. Lam, YW, Nelson CS, Sherman SM (2006) Mapping of the functional interconnections between thalamic reticular neurons using photostimulation. *J Neurophysiol* 96(5):2593–2600.

64. Landisman CE, Long MA, Beierlein M, Deans MR, Paul DL, Connors BW (2002) Electrical synapses in the thalamic reticular nucleus. *J Neurosci* 22(3):1002–1009.

65. Long MA, Landisman CE, Connors BW (2004) Small clusters of electrically coupled neurons generate synchronous rhythms in the thalamic reticular nucleus. *J Neurosci* 24(2):341-349.

66. Fuentealba P, Crochet S, Timofeev I, Bazhenov M, Sejnowski TJ, Steriade M (2004) Experimental evidence and modeling studies support a synchronizing role for electrical coupling in the cat thalamic reticular neurons in vivo. *Eur J Neurosci* 20(1):111-9.

67. Deleuze C, David F, Béhuret S, Sadoc G, Shin HS, Uebele VN, Renger JJ, Lambert RC, Leresche N, Bal T (2012) T-type calcium channels consolidate tonic action potential output of thalamic neurons to neocortex. *J Neurosci* 32(35):12228–12236.

68. Pospischil M, Toledo-Rodriguez M, Monier C, Piwkowska Z, Bal T, Frégnac Y, Markram H, Destexhe A (2008) Minimal Hodgkin-Huxley type models for different classes of cortical and thalamic neurons. *Biol Cybern* 99(4-5):427–441.

69. Yamada WM, Koch C, Adams PR (1989) Multiple channels and calcium dynamics. *Methods in Neuronal Modeling*, eds Koch C, Segev I (MIT Press, Cambridge, MA), pp 97–133.

70. Tsodyks MV, Markram H (1997) The neural code between neocortical pyramidal neurons depends on neurotransmitter release probability. *Proc Natl Acad Sci USA* 94(2):719–723.

71. Tsodyks MV, Pawelzik K, Markram H (1998) Neural networks with dynamic synapses. *Neural Comput* 10(4):821-835.

72. Pinault D, Smith Y, Deschênes M (1997) Dendrodendritic and axoaxonic synapses in the thalamic reticular nucleus of the adult rat. *J Neurosci* 17(9):3215-3233.

73. Cruikshank SJ, Urabe H, Nurmikko AV, Connors BW (2010) Pathway-specific feedforward circuits between thalamus and neocortex revealed by selective optical stimulation of axons. *Neuron* 65(2):230-45.

74. Hou G, Smith AG, Zhang ZW (2016) Lack of Intrinsic GABAergic Connections in the Thalamic Reticular Nucleus of the Mouse. *J Neurosci* 36(27):7246-7252.

75. Dayan P, Abbott LF (2005) Theoretical Neuroscience, revised edition (MIT Press, Cambridge, MA).

76. Shimizu K, Stopfer M (2013) Gap junction. *Curr Biol* 23(23):R1026-1031.

77. Chen C, Regehr WG (2003) Presynaptic modulation of the retinogeniculate synapse. *J Neurosci* 23(8):3130–3135.

78. Siegel A, Sapru HN (2015) Essential Neuroscience, Third Edition (Lippincott Williams & Wilkins, Baltimore).

79. Jones EG (1975) Some aspects of the organization of the thalamic reticular complex. *J Comp Neurol* 162(3):285-308.

80. Sohal VS, Huntsman MM, Huguenard JR (2000) Reciprocal inhibitory connections regulate the spatiotemporal properties of intrathalamic oscillations. *J Neurosci* 20(5):1735-1745.

81. Crabtree JW (1996) Organization in the somatosensory sector of the cat's thalamic reticular nucleus. *J Comp Neurol* 366(2):207-222.

82. Cox CL, Huguenard JR, Prince DA (1997) Nucleus reticularis neurons mediate diverse inhibitory effects in thalamus. *Proc Natl Acad Sci USA* 94(16):8854-8859.

83. Moore JW, Ramon F (1974) On numerical integration of the Hodgkin and Huxley equations for a membrane action potential. *J Theor Biol* 45(1):249–273.

84. R Core Team (2013) R: A language and environment for statistical computing (R Foundation for Statistical Computing, Vienna). URL http://www.R-project.org/.

85. Friedman J, Hastie J, Tibshirani R (2010) Regularization paths for generalized linear models via coordinate descent. *J Stat Softw* 33(1):1-22.

86. Herz AV, Gollisch T, Machens CK, Jaeger D (2006) Modeling single-neuron dynamics and computations: a balance of detail and abstraction. *Science* 314(5796):80-5.

87. McCormick DA, Pape HC (1980) Properties of a hyperpolarization-activated cation current and its role in rhythmic oscillation in thalamic relay neurones. *J Physiol (Lond)* 431:291-318.

88. Williams SR, Stuart GJ (2000) Action potential backpropagation and somato-dendritic distribution of ion channels in thalamocortical neurons. *J Neurosci* 20(4):1307-17.

89. Contreras D, Curró Dossi R, Steriade, M (1993) Electrophysiological properties of cat reticular thalamic neurones in vivo. *J Physiol* 470:273-94.

90. Destexhe A, Contreras D, Steriade M, Sejnowski TJ, Huguenard JR (1996) In vivo, in vitro, and computational analysis of dendritic calcium currents in thalamic reticular neurons. *J Neurosci* 16(1):169-85.

91. Crandall SR, Govindaiah G, Cox CL (2010) Low-threshold Ca^{2+} current amplifies distal dendritic signaling in thalamic reticular neurons. *J Neurosci* 30(46):15419-29.

92. Leresche N, Lightowler S, Soltesz I, Jassik-Gerschenfeld D, Crunelli V (1991) Low-frequency oscillatory activities intrinsic to rat and cat thalamocortical cells. *J Physiol* 441:155-74.

93. Spreafico R, Battaglia G, Frassoni C (1991) The reticular thalamic nucleus (RTN) of the rat: cytoarchitectural, Golgi, immunocytochemical, and horseradish peroxidase study. *J Comp Neurol* 304(3):478-90.

94. Lee SH, Govindaiah G, Cox CL (2007) Heterogeneity of firing properties among rat thalamic reticular nucleus neurons. *J Physiol (Lond)* 582(1):195-208.

95. Landau, ID, Egger R, Dercksen VJ, Oberlaender M, Sompolinsky H (2016) The impact of structural heterogeneity on excitation-inhibition balance in cortical networks. *Neuron* 92(5):1106-1121.

96. Cucchiaro JB, Bickford ME, Sherman SM (1991) A GABAergic projection from the pretectum to the dorsal lateral geniculate nucleus in the cat. *Neuroscience* 41(1):213-26.

97. Winer JA, Saint Marie RL, Larue DT, Oliver DL (1996) GABAergic feedforward projections from the inferior colliculus to the medial geniculate body. *Proc Natl Acad Sci USA* 93:8005–10.

98. Peruzzi D, Bartlett E, Smith PH, Oliver DL (1997) A monosynaptic GABAergic input from the inferior colliculus to the medial geniculate body in rat. *J Neurosci* 17:3766–77.

99. Llano DA, Slater BJ, Lesicko AM, Stebbings KA (2014) An auditory colliculo-thalamocortical brain slice preparation in mouse. *J Neurophysiol* 111:197–207.

100. Steriade M, Wyzinski P, Apostol V (1972) Corticofugal projections governing rhythmic thalamic activity. Corticothalamic Projections and Sensorimotor Activities, eds Frigyesi TL, Rinvik E, Yahr MD (Raven, New York), pp 221–72.

101. White EL, Hersch SM (1982) A quantitative study of thalamocortical and other synapses involving the apical dendrites of corticothalamic projection cells in mouse SmI cortex. *J Neurocytol* 11(1):137-57.

102. De Curtis M, Spreafico R, Avanzini G (1989) Excitatory amino acids mediate responses elicited in vitro by stimulation of cortical afferents to reticularis thalami neurons of the rat. *Neuroscience* 33(2):275-83.

103. Contreras D, Destexhe A, Sejnowski TJ, Steriade M (1996) Control of spatiotemporal coherence of a thalamic oscillation by corticothalamic feedback. *Science* 274(5288):771-4.

104. Blumenfeld H, McCormick DA (2000) Corticothalamic inputs control the pattern of activity generated in thalamocortical networks. *J Neurosci* 20(13):5153-62.

105. Zhang L, Jones EG (2004) Corticothalamic inhibition in the thalamic reticular nucleus. *J Neurophysiol* 91(2):759-66.

106. Crandall SR, Cruikshank SJ, Connors BW (2015) A corticothalamic switch: controlling the thalamus with dynamic synapses. *Neuron* 86(3):768-82.

107. Roy JP, Clercq M, Steriade M, Deschênes M (1984) Electrophysiology of neurons of lateral thalamic nuclei in cat: mechanisms of long-lasting hyperpolarizations. *J Neurophysiol* 51(6):1220-35.

108. Contreras D, Steriade M (1996) Spindle oscillation in cats: the role of corticothalamic feedback in a thalamically generated rhythm. *J Physiol* 490(1):159-179.

109. Suga N, Ma X (2003) Multiparametric corticofugal modulation and plasticity in the auditory system. *Nat Rev Neurosci* 4(10):783-94.

110. Sillito AM, Cudeiro J, Jones HE (2006) Always returning: feedback and sensory processing in visual cortex and thalamus. *Trends Neurosci* 29(6):307-16.

111. Muller L, Destexhe A (2012) Propagating waves in thalamus, cortex and the thalamocortical system: Experiments and models. *J Physiol Paris* 106(5-6):222-38.

112. Destexhe A, Sejnowski TJ (2003) Interactions between membrane conductances underlying thalamocortical slow-wave oscillations. *Physiol Rev* 83(4):1401-53.

113. Andersen P, Andersson SA (1968) The physiological basis of the alpha rhythm (Appleton-Century-Crofts, New York).

114. Jones EG (1985) The Thalamus (Plenum Press, New York).

115. Alonso JM, Usrey WM, Reid RC (2001) Rules of connectivity between geniculate cells and simple cells in cat primary visual cortex. *J Neurosci* 21(11):4002-15.

116. Miller LM, Escabí MA, Read HL, Schreiner CE (2001) Functional convergence of response properties in the auditory thalamocortical system. *Neuron* 32(1):151-60.

117. Rinzel J, Terman D, Wang X, Ermentrout B (1998) Propagating activity patterns in large-scale inhibitory neuronal networks. *Science* 279(5355):1351-5.

118. Steriade M, Llinás RR (1988) The functional states of the thalamus and the associated neuronal interplay. *Physiol Rev* 68(3):649-742.

119. Soltesz I, Lightowler S, Leresche N, Jassik-Gerschenfeld D, Pollard CE, Crunelli V (1991) Two inward currents and the transformation of low-frequency oscillations of rat and cat thalamocortical cells. *J Physiol (Lond)* 441:175-97.

120. Gibbs FA, Gibbs EL (1950) Atlas of Electroencephalography, volume one (Addison-Wesley, Cambridge, MA)

121. Bazhenov M, Timofeev I, Steriade M, Sejnowski TJ (1999) Self-sustained rhythmic activity in the thalamic reticular nucleus mediated by depolarizing $GABA_A$ receptor potentials. *Nat Neurosci* 2(2):168-74.

122. Bal T, Mccormick DA (1996) What stops synchronized thalamocortical oscillations? *Neuron* 17(2):297-308.

123. Lüthi A, McCormick DA (1998) Periodicity of thalamic synchronized oscillations: the role of Ca2+-mediated upregulation of Ih. *Neuron* 20(3):553-63.

124. Timofeev I, Bazhenov M, Sejnowski TJ, Steriade M (2001) Contribution of intrinsic and synaptic factors in the desynchronization of thalamic oscillatory activity. *Thalamus Relat Syst* 1(1):53-69.

125. Bonjean M, Baker T, Lemieux M, Timofeev I, Sejnowski T, Bazhenov M (2011) Corticothalamic feedback controls sleep spindle duration in vivo. *J Neurosci* 31(25):9124-34.

126. Huntsman MM, Porcello DM, Homanics GE, Delorey TM, Huguenard JR (1999) Reciprocal inhibitory connections and network synchrony in the mammalian thalamus. *Science* 283(5401):541-3.

127. Sohal VS, Huguenard JR (2003) Inhibitory interconnections control burst pattern and emergent network synchrony in reticular thalamus. *J Neurosci* 23(26):8978-88.

128. Crunelli V, Leresche N (2002) Childhood absence epilepsy: genes, channels, neurons and networks. *Nat Rev Neurosci* 3(5):371-82.

129. Lee SC, Patrick SL, Richardson, KA, Connors, BW (2014) Two functionally distinct networks of gap junction-coupled inhibitory neurons in the thalamic reticular nucleus. *J Neurosci* 34(39):13170-82.

130. Haas JS, Zavala B, Landisman CE (2011) Activity-dependent long-term depression of electrical synapses. *Science* 334(6054):389-93.

131. Haas JS, Landisman CE (2012) State-dependent modulation of gap junction signaling by the persistent sodium current. *Front Cell Neurosci* 5:31. doi:10.3389/fncel.2011.00031

132. Wang Z, Neely R, Landisman CE (2015) Activation of group I and group II metabotropic glutamate receptors causes LTD and LTP of electrical synapses in the rat thalamic reticular nucleus. *J Neurosci* 35(19):7616-25.

133. Kohmann D, Lüttjohann A, Seidenbecher T, Coulon P, Pape HC (2016) Short-term depression of gap junctional coupling in reticular thalamic neurons of absence epileptic rats. *J Physiol (Lond)* 594(19):5695-710.

134. Pernelle G, Nicola W, Clopath C (2017) Gap junction plasticity can lead to spindle oscillations. arXiv:1710.03999 [q-bio.NC]

135. Crabtree JW (2018) Functional Diversity of Thalamic Reticular Subnetworks. *Front Syst Neurosci* 12:41. doi:10.3389/fnsys.2018.00041

136. Scheibel ME, Scheibel AB (1966) The organization of the nucleus reticularis thalami: a Golgi study. *Brain Res* 1(1):43-62.

137. Spreafico R, De Curtis M, Frassoni C, Avanzini G (1988) Electrophysiological characteristics of morphologically identified reticular thalamic neurons from rat slices. *Neuroscience* 27(2):629-38.

138. Brunton J, Charpak S (1997) Heterogeneity of cell firing properties and opioid sensitivity in the thalamic reticular nucleus. *Neuroscience* 78(2):303-7.

139. Bickford ME (2016) Thalamic Circuit Diversity: Modulation of the Driver/Modulator Framework. *Front Neural Circuits* 9:86. doi: 10.3389/fncir.2015.00086

1499 **Figures:**

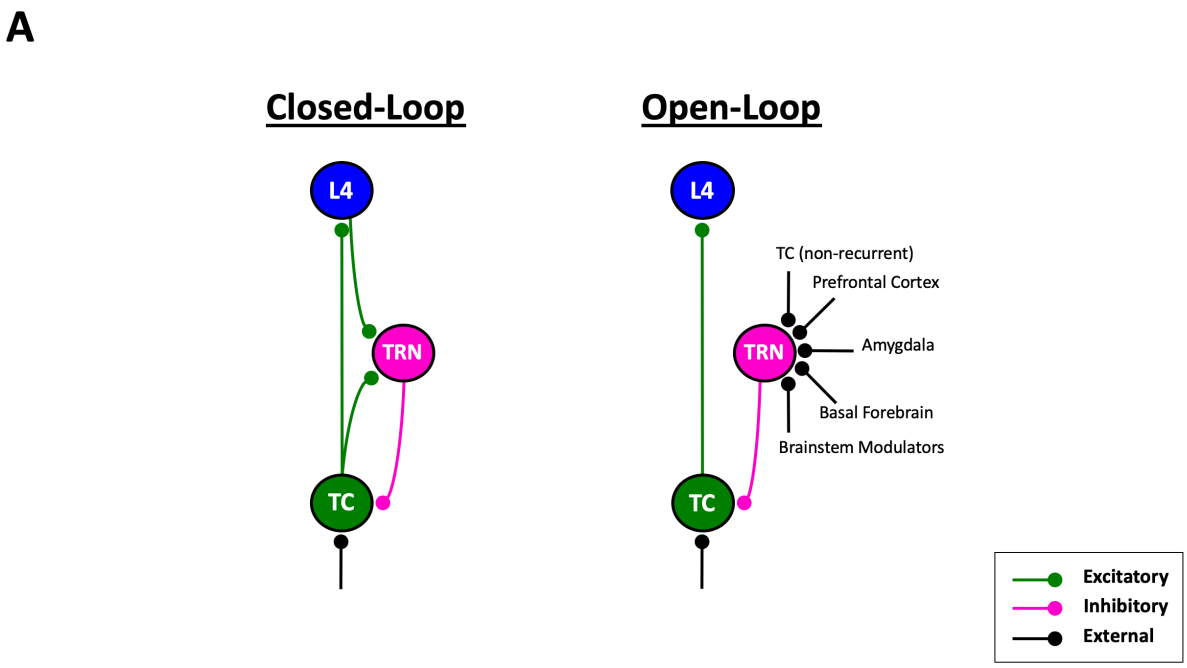

1500

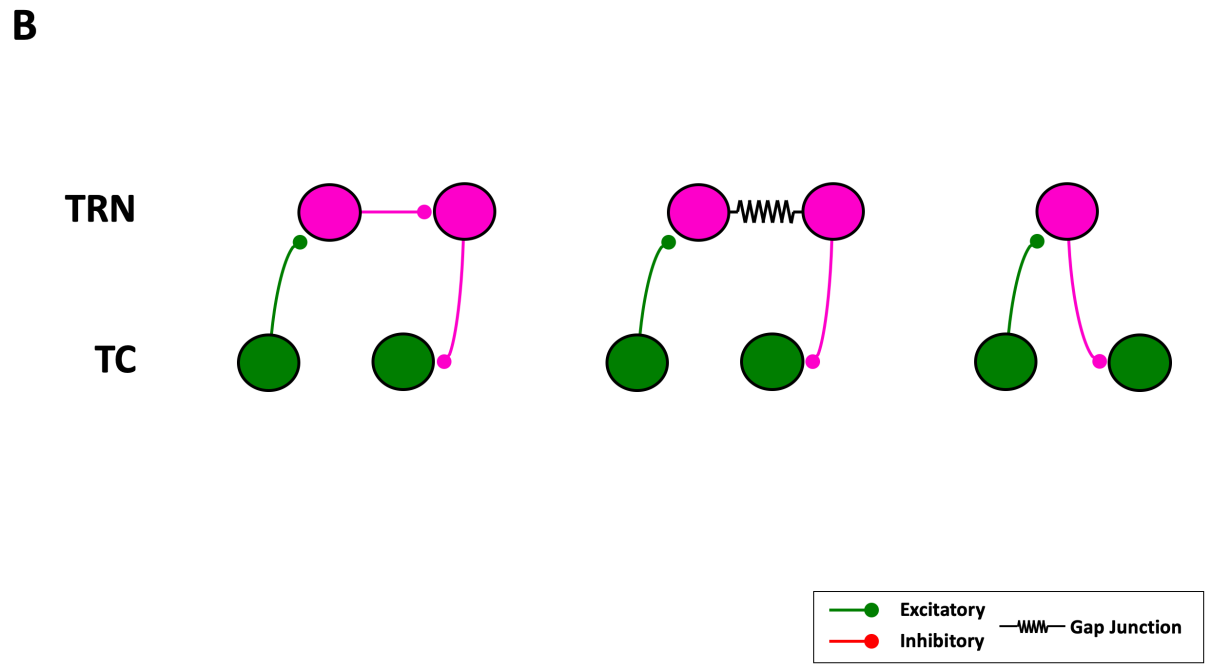

1501

1502 **Figure 1. A:** Closed- vs. open-loop thalamo-reticulo-thalamic configurations. **B:** Three possible pathways

1503 through which a signal might propagate from one thalamic relay (TC) neuron to another via the thalamic

1504 reticular nucleus (TRN).

A

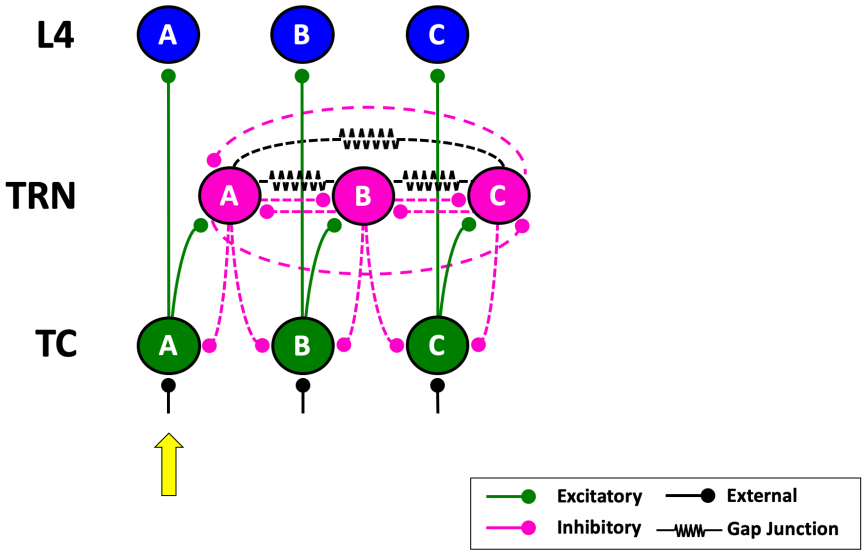

1505

B

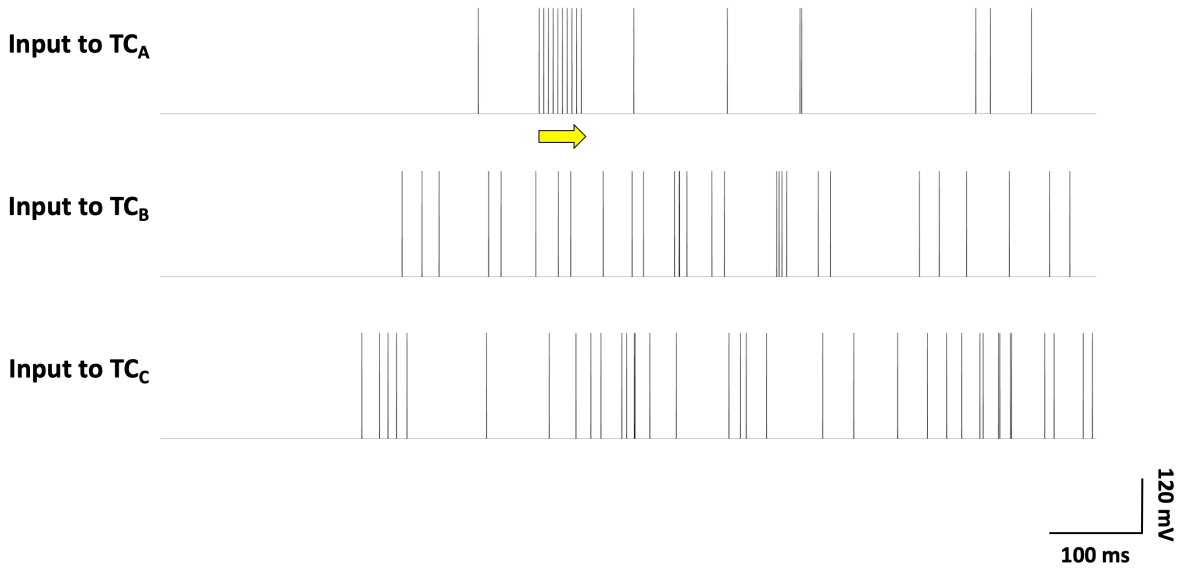

1506

Figure 2. A: Baseline three-layer, three-"column" thalamo-reticulo-cortical model network. Broken-line synapses were allowed to vary either as a class (homogeneously) or independently of one another (heterogeneously). **B,C:** Samples of the external input delivered to the TC neuron layer. TC_A received a combination of Poisson-modulated and fixed input, either punctate (B) or sustained (C).

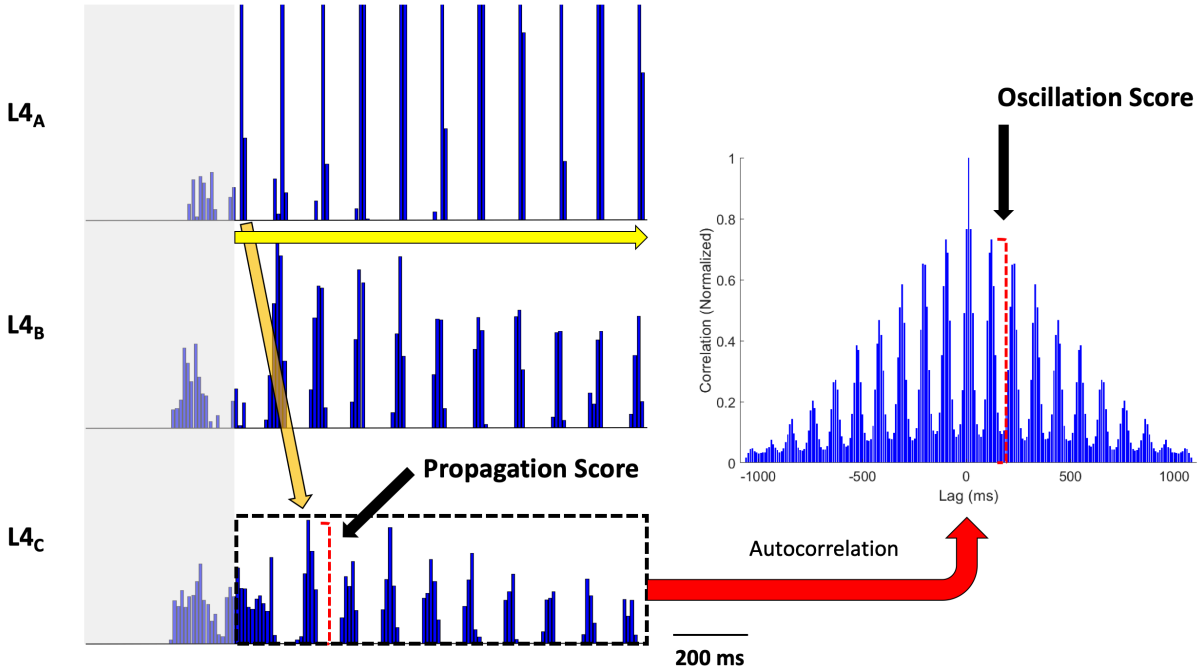

Figure 3. Sample detrended L4 spike histograms in a network permutation responding to a fixed, sustained stimulus delivered to TC_A (yellow arrow). The propagation score assigned to any network permutation was quantified as the amplitude of the initial stimulus-evoked response in the detrended $L4_c$ histogram; response propagation across the L4 subnetwork (orange arrow) was consistently linear, and thus the initial response in $L4_C$ was observed at a fixed interval relative to the onset of stimulation. Oscillation intrinsic to any network variant was quantified as the amplitude of the first off-center peak in the normalized autocorrelogram (right) of post-stimulation activity in the detrended $L4_C$ histogram (within broken black box). The initial 400 ms of activity preceding the fixed stimulus (in grey) is shown here for each histogram but was not included in the calculations of either propagation or oscillation. Note that the bin heights in the $L4_A$ histogram shown here were truncated in order to maintain identical vertical scaling across all three L4 histograms.

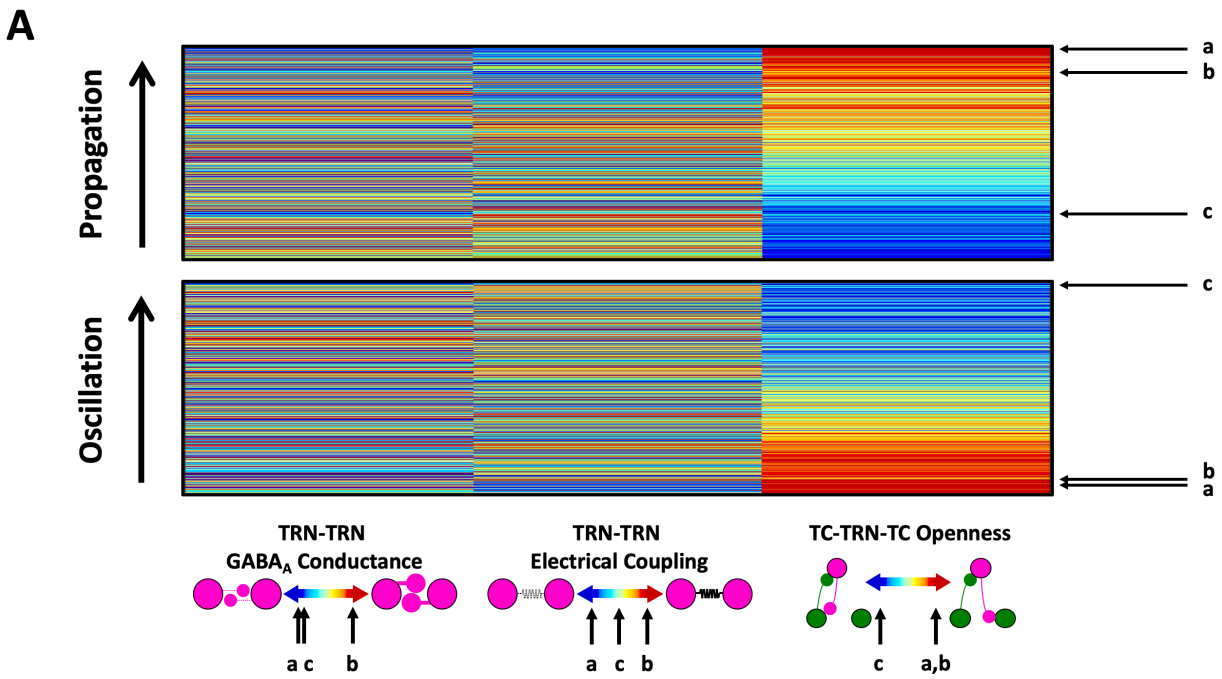

1537

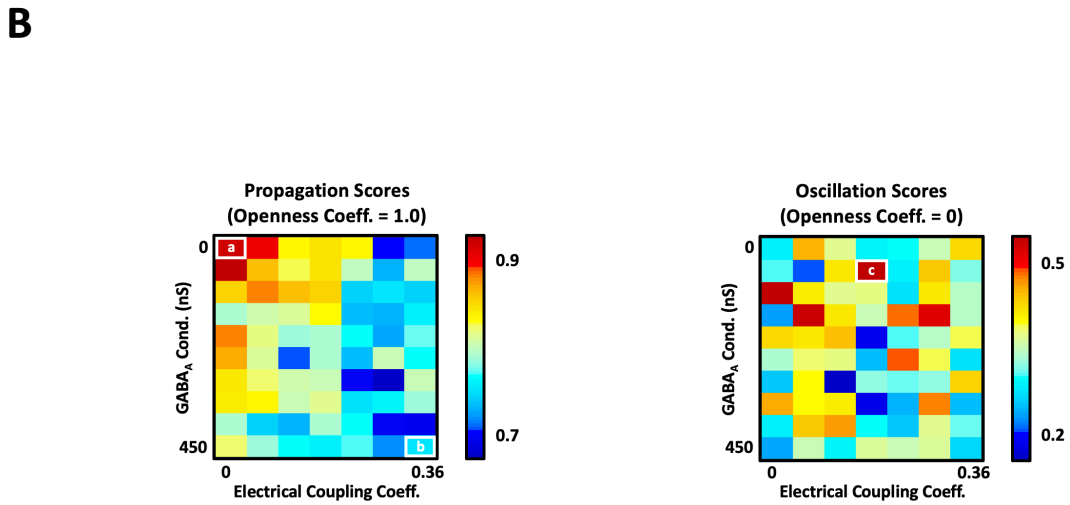

1538

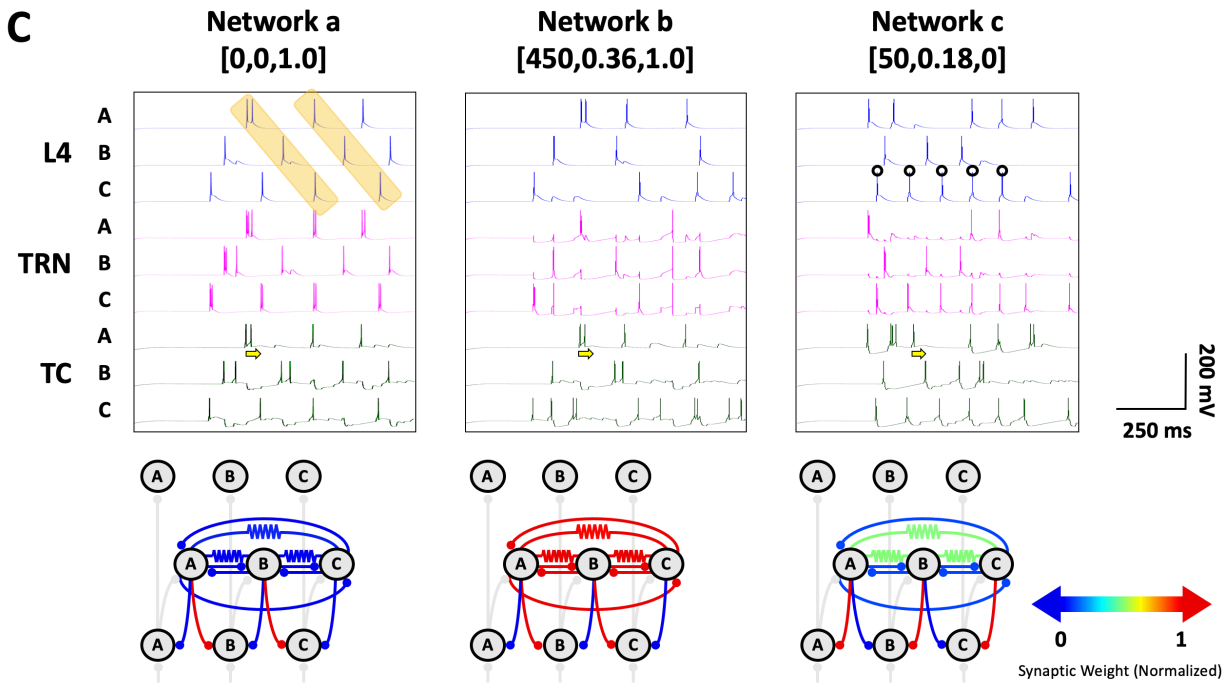

Figure 4. A: Ordinal heat maps ranking homogeneously synaptic network permutations according to the extent of supported signal propagation and oscillation in response to a fixed, punctate stimulus. Warmer colors correspond to higher values for each of the three synaptic class variables. The positions of three selected networks are indicated on both heat maps according to their propagation and oscillation scores. Each network is indexed by the synaptic variables ([TRN-TRN $GABA_A$ conductance (in nS), TRN-TRN electrical coupling coefficient, TC-TRN-TC openness coefficient]): a, [0,0,1.0]; b, [450,0.36,1.0]; and c, [50,0.18,0]. Networks with high degrees of TC-TRN-TC openness tended to best support signal propagation, while GABAergic synapses and electrical coupling between TRN neurons modestly impeded it. By contrast, networks with strong closed-loop reticulothalamic architectures were most permissive of oscillation, with TRN-TRN synaptic strength negligibly correlated with this property. **B:** Heat maps displaying propagation scores for the 70 fully open-loop homogeneously synaptic networks permutations (left, openness coefficient=1.0) and oscillation scores for the 70 fully closed-loop network permutations (right, openness coefficient=0), with the three selected networks indicated on the maps. Propagation was typically stronger in network permutations with minimal or nonexistent TRN-TRN connectivity (e.g., Network a, cf. Network b). **C:** Representative simulations and circuit diagrams

depicting the normalized synaptic makeups for each of the three selected networks. The yellow arrow indicates when the fixed, punctate stimulus was delivered to TC_A in each simulation. Orange highlighting indicates epochs of linear propagation, while circles are placed above spikes occurring during periods of oscillatory activity. Note that the episode of oscillatory activity depicted in the simulation of Network c changes frequency slightly following the third action potential.

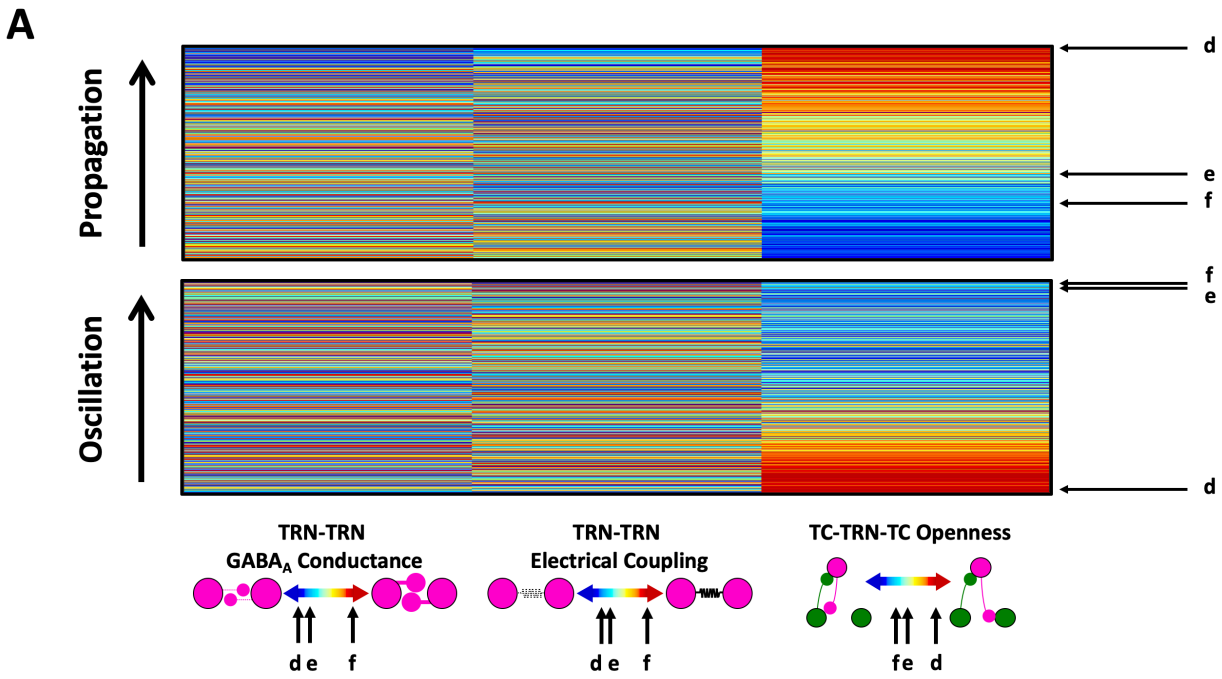

1581

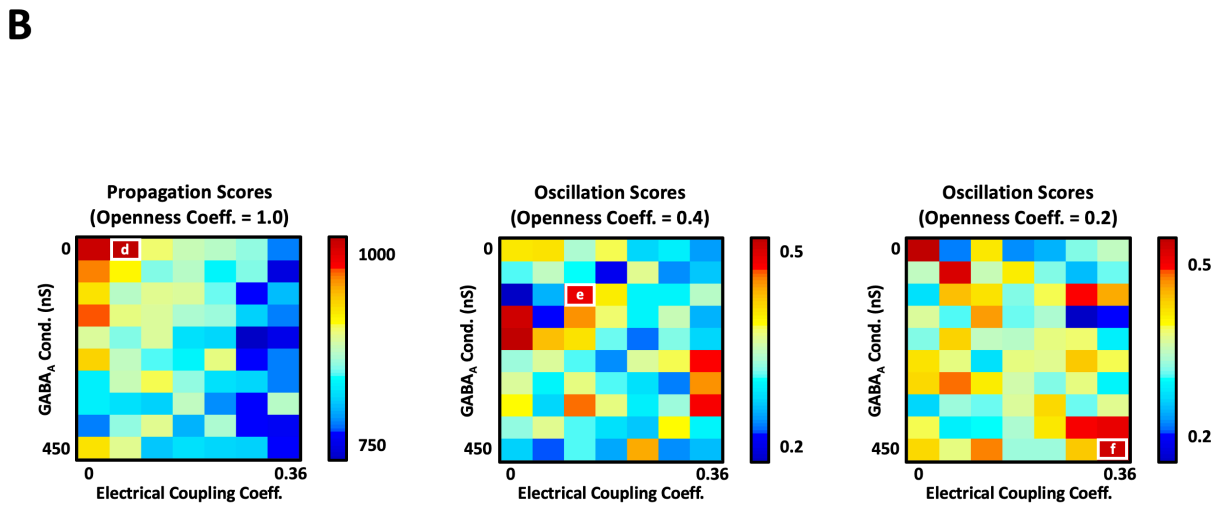

1582

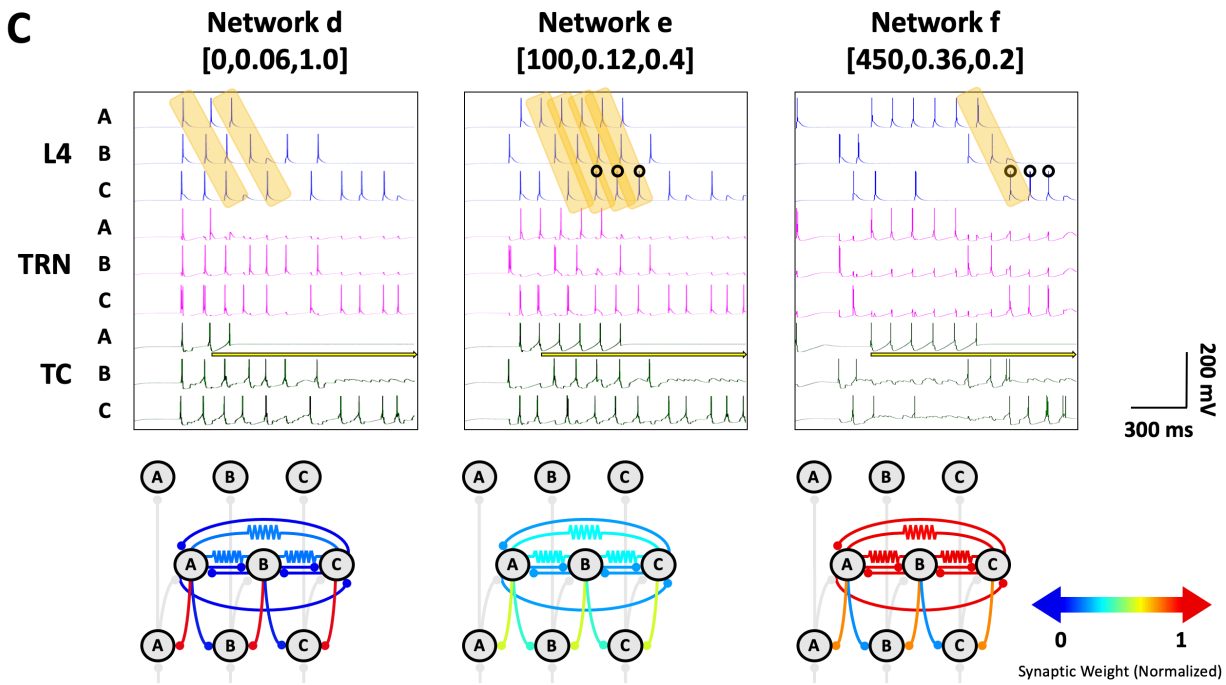

1583

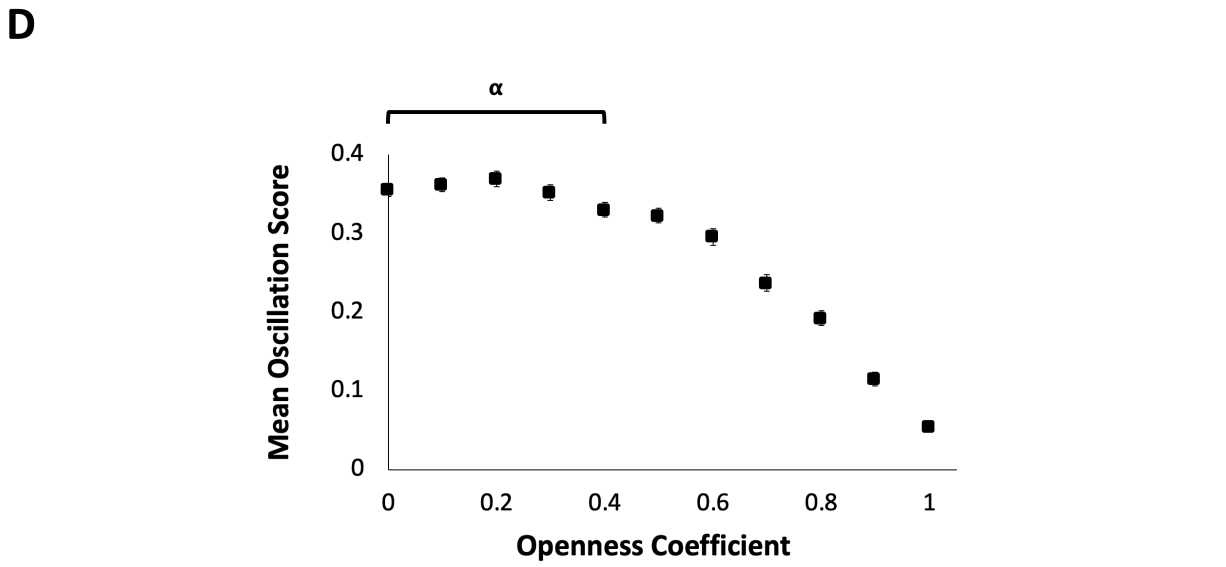

1584

1585 **Figure 5. A:** Ordinal heat maps ranking homogeneously synaptic network permutations according to the
1586 extent of supported signal propagation and oscillation in response to a fixed, sustained stimulus. The
1587 positions of three additional selected networks are indicated on both heat maps, with each selected
1588 network indexed as in Figure 4: d, [0,0.06,1.0]; e, [100,0.12,0.4]; and f, [450,0.36,0.2]. As was the case

with fixed, punctate stimulation, network propagation was strongest in networks exhibiting strong open-loop TC-TRN-TC connectivity, while the inverse was true with oscillation. Both varieties of TRN-TRN synapse tended to diminish propagation while exerting a negligible effect on oscillation. **B:** Heat maps displaying propagation and oscillation scores in TRN-TRN synaptic parameter space at different values of TC-TRN-TC openness, with the three selected networks indicated on the maps. Propagation was strongest in exclusively open-loop networks (left, openness coefficient=1.0), while oscillation was more likely to occur in networks with stronger closed-loop connectivity (middle, openness coefficient=0.4; right, openness coefficient=0.2). **C:** Representative simulations and circuit diagrams depicting the normalized synaptic makeups for each of the three additional selected networks. The yellow arrow indicates when the fixed, sustained stimulus was delivered to TC_A in each simulation. Note the two different mechanisms underlying oscillation in the simulations of Networks e and f. **D:** Mean oscillation scores for networks varied nonlinearly as a function of their openness coefficients, with networks possessing openness coefficients of 0 and 0.4 (α) supporting oscillation to equal extents (one-way ANOVA with Tukey post-hoc tests, $F(10,759)=137.8$, $p<0.0001$). Error bars indicate standard errors of the mean.

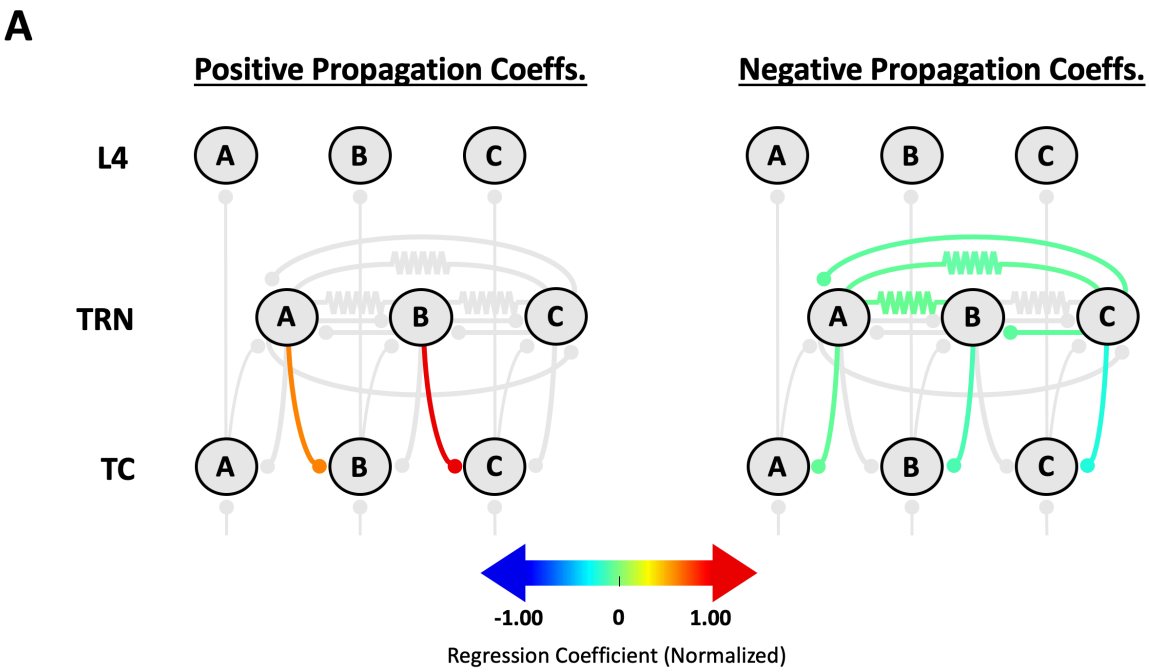

1615

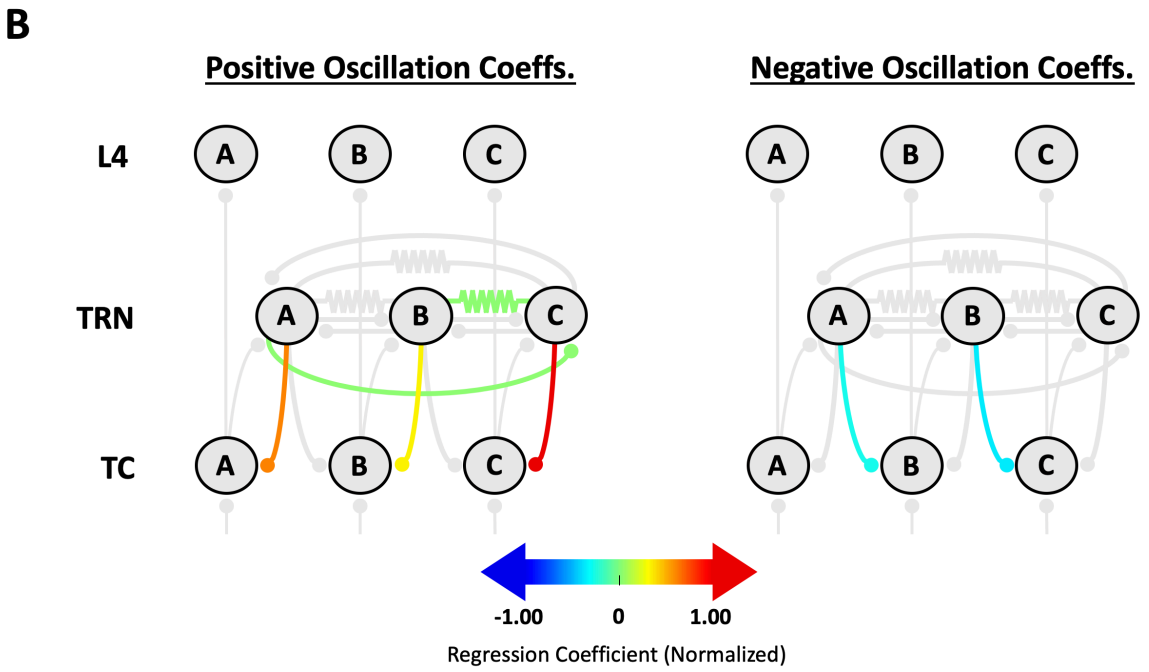

1616

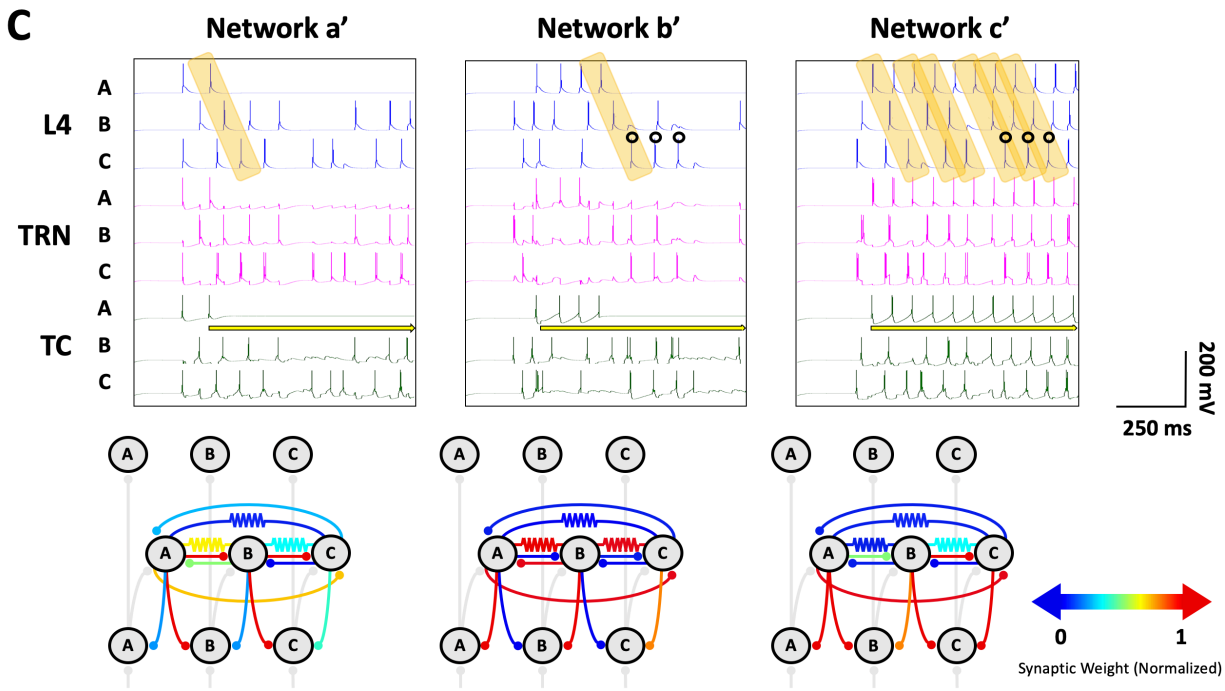

Figure 6. A,B: Network regression models illustrating how propagation (A) and oscillation (B) varied as a function of individual synaptic weights across simulated heterogeneously synaptic network permutations responding to a fixed, sustained stimulus delivered to TC_A. Gray synapses are either non-variable or associated with normalized regression coefficients with absolute values under 0.05. Synapses with positive and negative coefficients in the regression models are depicted separately in the left- and right-sided circuit diagrams, respectively. **C:** Representative simulations for three selected heterogeneous networks, whose normalized synaptic weights are depicted in the circuit diagrams. The yellow arrow indicates when the fixed, sustained stimulus was delivered to TC_A in each simulation. Networks a', b', and c' respectively illustrate propagation, self-contained generation of oscillation in network "Column C," and propagation of oscillation from Column A to Column C.

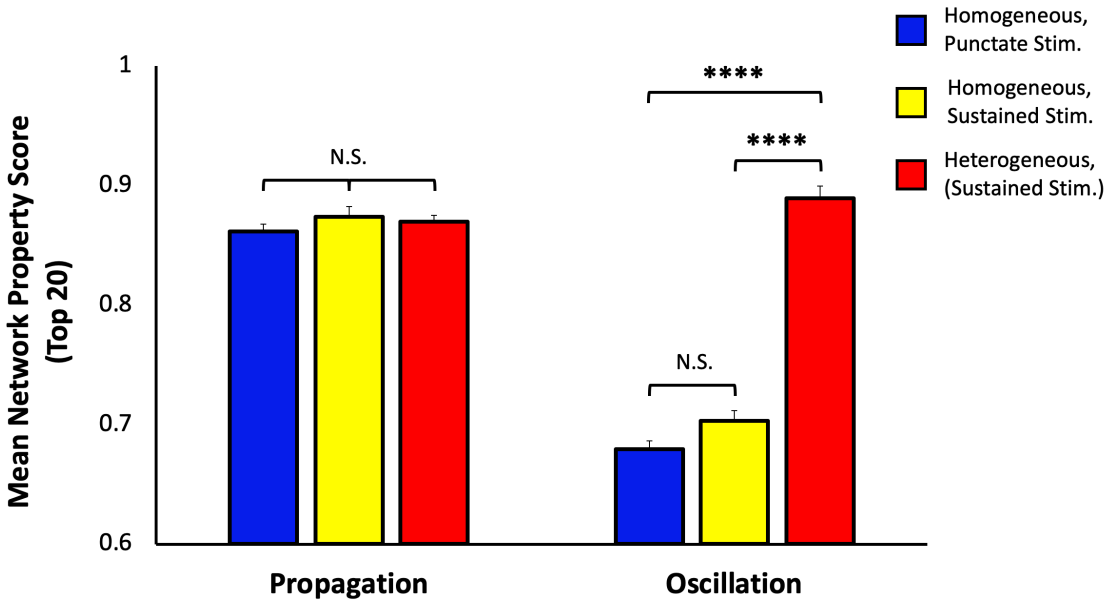

Figure 7. Propagation, as measured in those network permutations scoring highest with respect to the property, was equally supported in networks where synaptic weights varied independently of one another (**heterogeneously**; red) as in networks where synaptic strength varied **homogeneously** (blue, yellow) by class [one-way ANOVA, $F(2,59)=0.84$, $p=0.437$]. By contrast, oscillation scores were significantly higher in top-performing heterogeneous networks than their homogeneous counterparts [one-way ANOVA with Tukey's HSD tests, $F(2,59)=166.14$, $p<0.0001$], while there was no significant difference in oscillation among top-performing homogeneous network variants when stimulated externally in a fixed, punctate (blue) or sustained (yellow) manner (Tukey's test, $p=0.153$). Each bar corresponds to a mean of the top 20 network propagation or oscillation scores within each synaptic architecture/fixed stimulation group; error bars indicate standard errors of the mean. ****=Tukey's test, $p<0.0001$; N.S.=not significant.

Model Cellular Parameters			
Parameter	**TC cell**	**TRN cell**	**L4 cell**
Leak conductance, g_L (nS)	3.263	3.7928	4.8128
Leak reversal potential, E_L (mV)	-60.03	-57	-60.2354
Transient sodium conductance, g_{Na} (nS)	1,500	3,000	3,000
Sodium equilibrium potential, E_{Na} (mV)	50		
Delayed-rectifier potassium conductance, g_K (nS)	520	400	140
M-type potassium conductance, g_M (nS)	-	3.5	1.5
M-type potassium time constant, τ_M (ms)	-	200	180
Potassium equilibrium potential, E_K (mV)	-100		-90
T-type calcium conductance, g_T (nS)	45	21	-
Calcium equilibrium potential, E_T (mV)	120		
H-current conductance, g_H (nS)	0.608	0.0192	-
H-current reversal potential, E_H (mV)	-33		-
Membrane capacitance, C_m (pF)	100.4	75.0	109.3865

Table 1. Intrinsic model cellular parameters.

Model Synaptic Parameters						
Synapse	**Neurotransmitter**	**Conductance (nS)**	**τ_{recov} (ms)**	**τ_{inact} (ms)**	**Reversal Potential (mV)**	**U_{SE}**
External synapse to TC cell	(Glutamate)	32	125	2.64	0	0.76
TC-to-TRN cell synapse (TC-TRN)	Glutamate	150	500	2.64	0	0.76
TC-to-L4 cell synapse (TC-L4)	Glutamate	50	160	11.52	0	0.8113
TRN-to-TC cell synapse (TRN-TC)	$GABA_A$	Variable (0-80)	167.29	16.62	-80	0.62
Chemical TRN-to-TRN cell synapse ($TRN\text{-}TRN_{GABA}$)	$GABA_A$	Variable (0-450)	225	15	-75	0.62

Table 2. Model synaptic parameters. The external synapse to TC neurons, through which both fixed and stochastic inputs were delivered, was generically excitatory but explicitly modeled on glutamatergic retinogeniculate synapse (Chen and Regehr, 2003). The τ_{recov}, τ_{inact}, and U_{SE}, parameters derived from the synaptic depression model of Tsodyks and Markram (1997; Tsodyks et al., 1998), represent the time constant for post-exocytotic synaptic recovery, the time constant characterizing synaptic inactivation following the onset of presynaptic neurotransmitter release, and the fraction of available "resources" (synaptic vesicles) available for release at the presynaptic terminal following action potential induction. The conductances of both TRN-TC and $TRN\text{-}TRN_{GABA}$ synapses were allowed to vary within the specified ranges.

Normalized Regression Coefficients (NRCs)				
Synaptic Variable	**Propagation Linear**	**Propagation 2°**	**Oscillation Linear**	**Oscillation 2°**
$TRN\text{-}TRN_{GABA}$	-0.137	-0.413	0.058	-
$TRN\text{-}TRN_{Elec}$	-0.193	-0.499	0.064	0.056
TRN-TC	1.000	1.000	-1.000	-1.000
$(TRN\text{-}TRN_{GABA})^2$	-	0.117	-	-
$(TRN\text{-}TRN_{Elec})^2$	-	0.266	-	-
$(TRN\text{-}TC)^2$	-	0.213	-	-0.010
$TRN\text{-}TRN_{GABA}$ **x** $TRN\text{-}TRN_{Elec}$	-	0.226	-	-
$TRN\text{-}TRN_{Elec}$ **x** TRN-TC	-	-0.239	-	-

Table 3. Normalized linear and second-order regression coefficients for propagation and oscillation in homogeneously synaptic networks excited by a fixed, punctate stimulus. The regressions include 1°, 2°, and interaction terms corresponding to $TRN\text{-}TRN_{GABA}$, $TRN\text{-}TRN_{Elec}$, and open-loop TC-TRN-TC synapses/pathways. Terms associated with regression coefficients of absolute values < 0.05 are omitted. Positive and negative terms are highlighted in red and blue, respectively. Linear regression for propagation, R^2=0.829, RMSE=0.042, p<0.0001; second-order regression for propagation, R^2=0.863, RMSE=0.039, p<0.0001; linear regression for oscillation, R^2=0.661, RMSE=0.137, p<0.0001; second-order regression for oscillation, R^2=0.687, RMSE=0.132, p<0.0001.

Normalized Regression Coefficients (NRCs)				
Synaptic Variable	**Propagation Linear**	**Propagation 2°**	**Oscillation Linear**	**Oscillation 2°**
$TRN\text{-}TRN_{GABA}$	-0.173	-0.670	-	0.060
$TRN\text{-}TRN_{Elec}$	-0.136	-0.347	-	-
TRN-TC	1.000	1.000	-1.000	-0.052
$(TRN\text{-}TRN_{GABA})^2$	-	0.332	-	-
$(TRN\text{-}TRN_{Elec})^2$	-	0.164	-	-
$(TRN\text{-}TC)^2$	-	0.594	-	-1.000
$TRN\text{-}TRN_{GABA}$ **x** $TRN\text{-}TRN_{Elec}$	-	0.262	-	-
$TRN\text{-}TRN_{GABA}$ **x** TRN-TC	-	-0.152	-	-
$TRN\text{-}TRN_{Elec}$ **x** TRN-TC	-	-0.365	-	-

Table 4. Normalized linear and second-order regression coefficients for propagation and oscillation in homogeneously synaptic networks excited by a fixed, sustained stimulus. Linear regression for propagation, R^2=0.793, RMSE=0.047, p<0.0001; second-order regression for propagation, R^2=0.842, RMSE=0.041, p<0.0001; linear regression for oscillation, R^2=0.526, RMSE=0.145, p<0.0001; second-order regression for oscillation, R^2=0.630, RMSE=0.128, p<0.0001.

Normalized Regression Coefficients (NRCs)				
Synaptic Variable	Propagation Linear	Propagation 2°	Oscillation Linear	Oscillation 2°
TRN_A-TRN_C	-	-	0.115	-
TRN_C-TRN_A	-0.088			
TRN_C-TRN_B	-0.084	-0.073	-	-
TRN_A=TRN_B	-0.051	-0.091	-	-
TRN_A=TRN_C	-0.072	-	-	-
TRN_B=TRN_C	-	-0.113	0.117	-
TRN_A-TC_A	-0.075	-	0.621	0.077
TRN_A-TC_B	0.608	0.571	-0.289	-1.000
TRN_B-TC_B	-0.128	-0.196	0.333	0.417
TRN_B-TC_C	1.000	1.000	-0.379	-0.892
TRN_C-TC_C	-0.207	-0.239	1.000	0.107
$(TRN_C$-$TRN_B)^2$	-	0.079	-	-
$(TRN_A$-$TC_B)^2$	-	-0.245	-	0.189
$(TRN_B$-$TC_B)^2$	-	0.174	-	-0.093
$(TRN_B$-$TC_C)^2$	-	-0.472	-	0.278
$(TRN_C$-$TC_C)^2$	-	0.187	-	-0.146

Normalized Regression Coefficients (NRCs), continued		
Synaptic Variable	Propagation 2°	Oscillation 2°
TRN_A-TRN_B x TRN_A-TC_B	0.070	-
TRN_A-TRN_C x TRN_C-TC_C	-	0.215
TRN_B-TRN_A x TRN_A=TRN_B	-	0.111
TRN_B-TRN_A x TRN_A-TC_A	-	-0.186
TRN_C-TRN_A x TRN_A-TC_A	-	-0.172
TRN_C-TRN_A x TRN_A-TC_B	-0.119	-
TRN_C-TRN_A x TRN_B-TC_C	-0.096	-
TRN_C-TRN_B x TRN_B-TC_C	-0.153	-
TRN_A=TRN_B x TRN_B-TC_C	-	-0.129
TRN_A=TRN_C x TRN_A-TC_A	-	-0.114
TRN_A=TRN_C x TRN_C-TC_C	-0.079	-
TRN_A-TC_A x TRN_A-TC_B	-	0.634
TRN_A-TC_A x TRN_B-TC_C	-	0.449
TRN_A-TC_B x TRN_B-TC_B	-0.166	0.361
TRN_A-TC_B x TRN_B-TC_C	0.753	-0.274
TRN_A-TC_B x TRN_C-TC_C	-0.106	0.669
TRN_B-TC_B x TRN_B-TC_C	-	0.345
TRN_B-TC_B x TRN_C-TC_C	-	-0.192
TRN_B-TC_C x TRN_C-TC_C	-0.124	0.399

Table 5. Normalized linear and second-order regression coefficients for oscillation, propagation, and optimization in heterogeneously synaptic networks excited by a fixed, sustained stimulus. The regressions include 1°, 2°, and interaction terms corresponding to the 14 variable synapses in the networks. Equal signs denote gap junctions. Linear regression for propagation, R^2=0.742, RMSE=0.069, p<0.0001; second-order regression for propagation, R^2=0.857, RMSE=0.051, p<0.0001; linear regression for oscillation, R^2=0.253, RMSE=0.131, p<0.0001; second-order regression for oscillation, R^2=0.388, RMSE=0.118, p<0.0001.